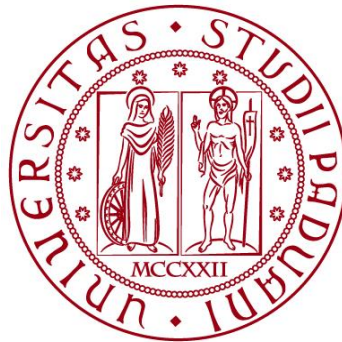


UNIVERSITÀ DEGLI STUDI DI PADOVA

DIPARTIMENTO DI BIOLOGIA

Corso di Laurea in Biologia Molecolare



ELABORATO DI LAUREA

**RUOLO DI DJ-1 NELLA MALATTIA DI PARKINSON:
CONTRIBUTO DEGLI ASTROCITI NEL PROCESSO DI
NEURODEGENERAZIONE**

**Tutor: Prof. Marco Bisaglia
Dipartimento di Biologia**

**Co-tutor: Dott. Francesco Agostini
Dipartimento di Biologia**

Laureando: Giosuè Bovo

ANNO ACCADEMICO 2023/2024

Indice

ABSTRACT

1. INTRODUZIONE: DJ-1 E MALATTIA DI PARKINSON.....	1
1.1 FUNZIONI DELLA PROTEINA DJ-1.....	1
1.2 EFFETTI DELLA MALATTIA DI PARKINSON	2
1.3 AUTOFAGIA	3
1.4 OBIETTIVI DEL LAVORO	4
2. MATERIALI E METODI.....	6
2.1 IMMUNOISTOCHEMICA.....	6
2.2 WESTERN BLOT E DOT BLOT.....	6
2.3 ORGANOIDI DI MESENCEFALO E COLTURE DI ASTROCITI.....	7
2.4 SAGGIO SEAHORSE XF	9
2.5 SAGGIO QUANTITATIVO DQ RED BSA	9
2.6 ANALISI PROTEOMICA GLOBALE E FOSFOPROTEOMICA.....	10
3. RUOLO DI DJ-1 IN ORGANOIDI UMANI DI MESENCEFALO	11
3.1 ORGANOIDI DJ-1-KO DIMOSTRANO DISFUNZIONI AUTOFAGICHE E ACCUMULO DI α -SINUCLEINA	11
3.2 ORGANOIDI DJ-1-KO ACCUMULANO PROTEINE DANNEGGIATE DA GLICAZIONE.....	14
4. RUOLO DI DJ-1 NEGLI ASTROCITI	17
4.1 LA PERDITA DI FUNZIONE DI DJ-1 INDUCE NEUROTOSSICITÀ.....	17
4.2 MECCANISMI CELLULARI COINVOLTI NELLA PERDITA DI FUNZIONE DI DJ-1	18
4.3 LA PERDITA DI FUNZIONE DI DJ-1 NEGLI ASTROCITI COMPROMETTE I LISOSOMI PORTANDO ALL'ACCUMULO DI α -SINUCLEINA.....	20
5. CONCLUSIONI E DISCUSSIONE.....	24

BIBLIOGRAFIA

APPENDICE

ABSTRACT

DJ-1 è una proteina che gioca un ruolo cruciale nel mantenimento delle funzioni mitocondriali e, in generale, dell'omeostasi cellulare. A livello neuronale, l'importanza di DJ-1 è confermata dal fatto che le mutazioni che determinano perdita della funzione di questa proteina sono causa di una rara forma genetica recessiva della malattia di Parkinson (PD). Coerentemente, attraverso l'utilizzo di organoidi di mesencefalo derivati da cellule staminali pluripotenti indotte (iPSC) è stato dimostrato che la perdita della funzione di DJ-1 causa una riduzione della proteolisi lisosomiale. Questo difetto favorisce un aumento dei livelli di α -sinucleina sia in forma fosforilata che aggregata e un accumulo di *advanced glycation end products* (AGEs) nelle biomolecole, entrambi fenotipi riconducibili allo sviluppo di PD. Il lavoro scientifico analizzato evidenzia il ruolo cruciale degli astrociti nel rimuovere proteine aggregate o tossiche, proteggendo così la funzione neuronale. Come dimostrato in co-culture di neuroni di mesencefalo e astrociti, nelle cellule gliali, DJ-1 partecipa al mantenimento dell'attività proteolitica assicurando una corretta proteostasi dei neuroni. Al contrario, astrociti DJ-1 *loss of function* acquisiscono un fenotipo infiammatorio e perdono la loro funzione protettiva. In conclusione, la perdita di funzione di DJ-1 non solo impedisce agli astrociti di evitare l'accumulo proteico tossico che porta a neurodegenerazione in modelli di PD, ma lo favorisce.

1. INTRODUZIONE: DJ-1 E PARKINSON

DJ-1 è una piccola proteina omodimerica, codificata dal gene *PARK7*, evolutivamente molto conservata tra procarioti e eucarioti(1,2). È espressa in modo ubiquitario e localizzata principalmente nel citoplasma, ma viene anche trasferita nel nucleo e nei mitocondri in condizioni di stress(3,4). Il suo corretto livello di espressione è fondamentale per il mantenimento dell'omeostasi cellulare. Infatti, la sovraespressione di DJ-1 può essere correlata alla progressione di forme di cancro(3), mentre la perdita della sua funzione è associata a malattie neurodegenerative. Mutazioni in omozigosi nel gene *PARK 7* sono correlate a forme recessive della malattia di Parkinson (PD) (5).

1.1 FUNZIONI DELLA PROTEINA DJ-1

Le funzioni di questa proteina sono molteplici ma i meccanismi molecolari attraverso cui agisce non sono ancora del tutto chiari. DJ-1 è coinvolta nell'omeostasi e nella respirazione mitocondriale, prevenendo l'incremento di ROS(6,7). L'assenza di DJ-1 causa la frammentazione dei mitocondri e porta ad una riduzione del loro potenziale di membrana in varie linee cellulari, tra cui neuroni dopaminergici umani(6,7). Tramite saggi di co-immunoprecipitazione si è scoperto che DJ-1 interagisce con le subunità β dell'ATP-sintetasi mitocondriale e con le due subunità del complesso I mitocondriale. In neuroni dopaminergici murini la perdita di funzione del complesso I è associata a difetti nel suo assemblaggio, che è ritenuto sia proprio mediato da DJ-1(8). Questa proteina è inoltre coinvolta nella corretta modulazione del processo di mitofagia, un meccanismo cellulare mediante il quale vengono degradati i mitocondri(7,9).

È noto che DJ-1 abbia anche un'importante proprietà antiossidante e che possa essere considerata un sensore di ROS. In particolare, le interazioni di DJ-1 con proteine mitocondriali aumentano in condizioni di stress ossidativo, suggerendo che una delle funzioni della proteina sia coinvolta nella risposta contro l'iperossidazione(10,11). Il silenziamento di questa proteina causa ipersensibilità allo stress ossidativo e morte cellulare indotta da ROS(4,12,13). DJ-1 presenta tre residui di cisteina conservati: Cys43, Cys53 e Cys106, suscettibili a modificazioni post-traduzionali in risposta alla variazione dello stato ossidativo nella cellula. L'ultimo residuo in particolare ha un ruolo

essenziale nella funzione antiossidante della proteina, che viene persa se Cys106 viene sostituito con serina, alanina o aspartato(14). Questo residuo può essere ossidato consecutivamente in tre forme. La forma sulfonica (SO₃H) è la forma attiva di DJ-1 che partecipa alle funzioni antiossidanti. Un'eccessiva ossidazione di questa proteina, tuttavia, la destabilizza fino alla perdita di funzione(15). Sono stati svolti vari studi per comprendere i meccanismi molecolari tramite cui DJ-1 svolge la sua funzione antiossidante, finora però non si è giunti a una risposta univoca. *In vitro*, DJ-1 sembra svolgere un'attività di *scavenging* diretta eliminando il perossido di idrogeno (12), inoltre regola l'espressione di fattori di trascrizione come Nrf2, coinvolto a sua volta nella modulazione di geni antiossidanti(16). DJ-1 sembra essere anche coinvolta nell'attivazione dell'enzima antiossidante *Copper-Zinc Superoxide Dismutasi 1* (SOD1) tramite trasporto di ioni rame (17). Questa sua funzione non è tuttavia universalmente accettata, dal momento che alcuni lavori sostengono che l'attività di DJ-1 sia esercitata indipendentemente dalla presenza di SOD1(18).

La funzione di DJ-1 è stata infine associata anche al processo dell'autofagia (*Autophagy Lysosomal Pathway - ALP -*), un meccanismo di degradazione cellulare che verrà descritto in seguito. Infatti, in cellule di neuroblastoma il silenziamento di DJ-1 riduce i livelli di *microtubule-associated protein 1A/1B light chain 3* (LC3), una proteina coinvolta nel processo autofagico che si localizza nella membrana dell'autofagosoma. Inoltre, l'assenza di DJ-1 causa l'iperattivazione di *mechanistic target of rapamycin 1* (mTORC1), un complesso proteico con azione inibente nei confronti dell'autofagia(19). Il silenziamento di DJ-1 è stato infine recentemente associato a disfunzioni dell'autofagia nella microglia, dove favorisce l'accumulo di proteine, tra cui α -sinucleina(20).

1.2 EFFETTI DELLA MALATTIA DI PARKINSON

Dal momento che DJ1 ha importanti funzioni antiossidanti e di regolazione dell'autofagia è comprensibile come possa essere correlata ai processi che accompagnano lo sviluppo della PD. Questa patologia causa la morte cellulare di una precisa popolazione neuronale della *substantia nigra* (SN), i neuroni dopaminergici. Le cause di questa patologia possono essere sia ambientali che genetiche. Oltre a

PARK7, sono stati identificati diversi geni la cui mutazione è causa di forme familiari di PD. Si tratta di forme autosomiche recessive - tra cui appunto *PARK7*, *parkin* e *pink1* - ma anche forme autosomiche dominanti, tra le quali è presente il gene *SNCA* (codificante α -sinucleina)(21). Proprio mutazioni a quest'ultimo gene sono associate a disfunzioni nell'autofagia e a meccanismi di controllo della qualità proteica, condizioni che promuovono l'accumulo di specie tossiche di α -sinucleina, come la forma fosforilata e aggregata (22). Un altro processo associato a PD è l'accumulo cellulare di AGEs. Queste sono molecole che si generano a causa della glicazione di lipidi e proteine da parte di zuccheri. L'accumulo di AGEs è un processo che accompagna l'invecchiamento, ma il suo eccessivo incremento è stato associato a malattie neurodegenerative correlate all'invecchiamento(23).

1.3 AUTOFAGIA

L'autofagia è un meccanismo che permette la degradazione e il riciclo di materiale intracellulare. Essa rappresenta uno strumento necessario alla cellula per un corretto turnover molecolare, per la rimozione di cargo specifici e per la degradazione di organelli. Questo importante processo avviene grazie alla formazione di autofagosomi, vescicole costituite da una doppia membrana che si generano dall'espansione del fagoforo, una struttura che origina nei siti di contatto tra reticolo endoplasmatico (RE) e mitocondrio(24–26). All'interno di essi viene reclutato il materiale che verrà digerito in seguito grazie all'attività dei lisosomi, organelli delimitati da membrana caratterizzati da un lume acido e dalla presenza di enzimi idrolitici, aventi il compito di degradare molecole biologiche. Il tasso di formazione degli autofagosomi, la loro grandezza e numero è essenziale per determinare la velocità e il livello di degradazione proteica nella cellula. Per la formazione del fagoforo vengono reclutate molte proteine facenti parte della famiglia *Autophagy Related Genes* (ATG)(27). La proteina ATG8, altrimenti detta LC3, è presente in maniera ubiquitaria nel citoplasma della cellula in forma non lipidata (LC3-I). Quando l'autofagia viene indotta, LC3-I viene reclutata nella membrana del fagoforo e lega il gruppo aminico della fosfatidiletanolamina. In questo modo viene convertita nella forma lipidata LC3-II(28). Il livello di LC3-II è quindi un indice per misurare il flusso autofagico e la sua alterazione in particolari condizioni.

Un'altra proteina utilizzata nell'analisi dell'autofagia è P62, un importante recettore che coadiuva la degradazione di aggregati e di substrati specifici favorendone l'inclusione nell'autofagosoma in formazione. Il suo corretto turnover rispecchia una proteostasi attiva(29). Ciò significa che la sua degradazione correla con il livello di attività lisosomiale. La funzionalità dei lisosomi infine può essere valutata attraverso saggi che analizzano l'attività di enzimi lisosomiali, uno di questi è la glucocerebrosidasi lisosomiale codificata dal gene *GBA1*. Questo enzima è necessario per la degradazione di glucosilceramidi e una sua disfunzione porta alla formazione di lisosomi anomali, all'accumulo di α -sinucleina e ad anomalie autofagiche(30).

I livelli delle proteine LC3-II e P62 vengono spesso utilizzati per indagare l'attività autofagica cellulare. Entrambi questi marcatori possono descrivere il flusso autofagico solo in modo parziale, per questo vengono misurati parallelamente. La variazione di LC3-II infatti fornisce informazioni solo sull'aumento o sulla diminuzione del numero di autofagosomi, ma non permette di analizzare l'attività degradativa autofagica. Il livello di P62 invece è associato più specificatamente alla proteolisi lisosomiale, ma il suo livello è influenzato anche da altri processi cellulari.

1.4 OBIETTIVI DEL LAVORO

In questo lavoro di tesi ho analizzato un articolo scientifico volto ad indagare il contributo degli astrociti nel processo di neurodegenerazione, prestando particolare attenzione agli effetti negativi che comporta la perdita di funzione di DJ-1 in questo tipo cellulare. Questa proteina, come già descritto, può svolgere diverse funzioni direttamente coinvolte nelle disfunzioni caratteristiche del PD: DJ-1 è coinvolto nei *pathways* dello stress ossidativo, in particolare nell'ossidazione della dopamina e ha un ruolo nella regolazione dell'autofagia(31). Inoltre, studi recenti hanno descritto l'attività glicosilasica di DJ-1, che protegge le macromolecole cellulari da glicazioni dannose(32-34). È stato anche osservato un aumento delle forme altamente ossidate e quindi inattive di DJ-1 nella corteccia cerebrale di pazienti PD(35). Tutto ciò conferma che la diminuzione dell'attività di questa proteina può contribuire alla patogenesi di PD.

Il lavoro scientifico analizzato descrive inizialmente gli effetti che la perdita di funzione di DJ-1 determina in modelli di organoidi umani. In particolare, viene indagata la correlazione tra l'assenza di DJ-1 e fenotipi associati a PD come l'accumulo di α -sinucleina e l'incremento di AGEs intracellulare. Lo studio si propone di analizzare in particolare il ruolo che gli astrociti hanno nella comparsa di questi fenotipi mediante l'utilizzo di colture 2D di queste cellule gliali. Attraverso un'analisi proteomica e fosfoproteomica degli astrociti, vengono inoltre descritti i processi molecolari significativamente influenzati dalla perdita di funzione di DJ-1. L'obiettivo dello studio è quindi quello di investigare, mediante l'utilizzo di diversi saggi, come le funzioni metaboliche vengano compromesse dalla mutazione del gene *PARK7*, in modo tale da chiarire il ruolo patogenico degli astrociti in PD.

2. MATERIALI E METODI

2.1 IMMUNOISTOCHEMICA

L'immunoistochimica è una tecnica che permette di evidenziare la presenza di specifiche proteine in sezioni di tessuto o in cellule fissate. Nello studio, analisi di questo tipo sono state svolte sia in cellule che in sezioni di organoidi.

Le cellule sono state fissate in paraformaldeide (PFA) 4% per 20 minuti. Per la preparazione del campione è stata usata una soluzione con 0,1% Triton X-100 - che permeabilizza le cellule permettendo così l'ingresso degli anticorpi - e siero equino 5% per il bloccaggio. Infine, le cellule sono state lavate in un buffer salino (PBS) e incubate *overnight* a 4°C con anticorpo primario specifico per la proteina di interesse. Dopo ulteriori lavaggi le cellule sono state incubate con anticorpi secondari coniugati a fluorofori che si legano all'anticorpo primario. Per la colorazione del nucleo i campioni sono stati incubati con DAPI, un intercalante del DNA.

Gli organoidi sono stati invece fissati in PFA 4% e inclusi in paraffina. Attraverso un microtomo sono state ottenute sezioni di 4-6 μm , poi mantenute *overnight* a 70°C. A seguire sono stati esposti gli antigeni mediante incubazione con acido citrico. Infine, le sezioni sono state incubate con anticorpo primario e secondario.

2.2 WESTERN BLOT E DOT BLOT

Il *western blotting* e il *dot blotting* sono due tecniche che permettono di analizzare il livello di specifiche proteine all'interno di un campione. Queste tecniche sono state largamente utilizzate nello studio, al fine di confrontare l'espressione di determinate proteine tra campioni con diverso genotipo sottoposti a trattamenti differenti.

Per ottenere i lisati a partire da colture cellulari o organoidi sono stati utilizzati un buffer RIPA e un buffer di lisi 1-2% SDS contenente gli inibitori delle proteasi e fosfatasi. La concentrazione proteica del lisato è stata misurata tramite metodo BCA. 20-40 μg di proteine denaturate e in condizioni riducenti sono stati caricati in gel elettroforetico

precasted. Le proteine attraversano il gel per differenza di potenziale a una velocità che dipende dalla loro carica e dimensione (proteine più piccole attraversano il gel più velocemente rispetto alle quelle di dimensioni maggiori). Le proteine sono state poi trasferite su membrane PVDF mediante un *dry blotting system*, che sfrutta la carica elettrica delle proteine per farle migrare grazie ad una differenza di potenziale. Le membrane sono state prima bloccate in soluzione di PBS contenente 5% di latte e 0,1% di Tween-20, poi lavate quattro volte in TBS-T ed infine incubate *overnight* con apposito anticorpo primario. Dopo quattro ulteriori lavaggi, le membrane sono state incubate con anticorpi secondari specie-specifici coniugati a perossidasi di rafano. Le proteine vengono visualizzate sottoforma di bande che si sviluppano tramite l'utilizzo di un substrato che reagisce con la perossidasi. La dimensione e l'intensità di colore di ogni banda correla con il livello di proteina nel campione.

È stato eseguito *stripping* per incubare le stesse membrane con anticorpi primari diversi. I *dot blot* sono stati ottenuti alla stessa maniera, senza però la necessità di separare in bande le proteine tramite una corsa elettroforetica in gel.

2.3 ORGANOIDI DI MESENCEFALO E COLTURE DI ASTROCITI

Per ottenere organoidi umani di mesencefalo (hMIDOs) sono state utilizzate *human induced pluripotent stem cells* (hiPSCs). Queste sono state coltivate in Stemflex™ medium a 37°C con 5% di CO₂ in incubatore umido. Per l'aggregazione e il differenziamento di organoidi sono state usate delle fiasche da 125 ml, posizionate in una piastra per mescolamento alla velocità di 65 rpm. Una volta che le sfere hanno raggiunto i 300-500 µm, condizione validata grazie ad opportuno filtraggio, è stato indotto il differenziamento mediante un cocktail di fattori. Per il mantenimento a lungo termine, gli organoidi sono stati trasferiti in piastre a bassa adesione alla concentrazione di 5 sfere per ml di terreno.

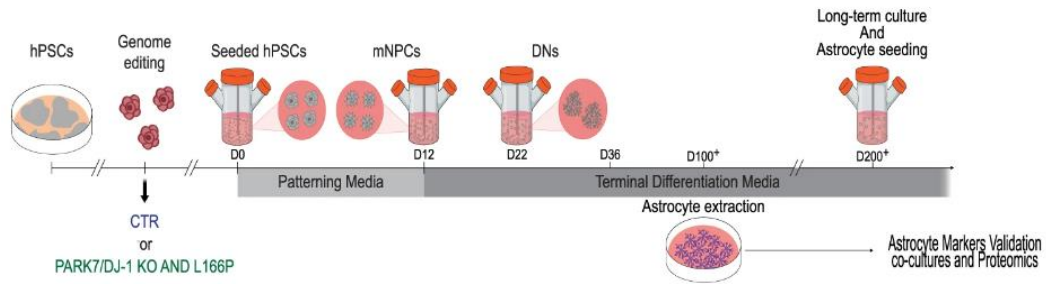


figura 1: viene descritto il processo di formazione degli organoidi a partire da hiPSCs umane. Gli hMIDO possono essere generati da linee cellulari di controllo o mutanti per DJ1. Il differenziamento avviene in due fasi, la seconda, a partire dal giorno 12, avviene grazie ad un terreno contenente fattori per il differenziamento del mesencefalo. Al giorno 100 è possibile generare delle colture di astrociti a partire dagli organoidi

Nello studio sono state ottenute colture bidimensionali di astrociti a partire dagli organoidi. Al giorno 90 le fiasche da 125 ml contengono centinaia di organoidi. Questi sono costituiti da diversi tipi cellulari: neuroni, tra cui i dopaminergici, cellule neurali progenitrici (NPCs) e cellule gliali, tra cui gli astrociti. Per isolare i progenitori degli astrociti, gli organoidi sono stati delicatamente spezzettati in soluzione di tripsina grazie ad una pipetta di vetro. Dopo lavaggi e centrifugazioni preliminari, le sospensioni cellulari sono state seminate in piastre da 15 cm in terreno semisolido. Le cellule sono state mantenute per una settimana in un terreno per la proliferazione degli astrociti, fino a quando i primi astrociti hanno aderito e hanno cominciato a dividersi. Al raggiungimento del 70% di confluenza, le colture sono state passate in nuove piastre. Per gli esperimenti di co-cultura, NPCs di mesencefalo di 14 giorni e astrociti di 100 giorni sono stati seminati in proporzione 5:1 in una piastra da 96 pozzetti. Le co-culture sono state mantenute in coltura per due settimane in medium di maturazione, per poi essere trasferite in terreno apposito per il mantenimento a lungo termine. Il protocollo di trapianto di astrociti in organoidi, invece, prevede che ad ogni hMIDO vengano inserite 50 mila cellule gliali. Per 72 ore la sospensione di organoidi è stata trattata con siero al fine di favorire l'impianto. Infine, ogni organoide è stato inserito in un pozzetto diverso.

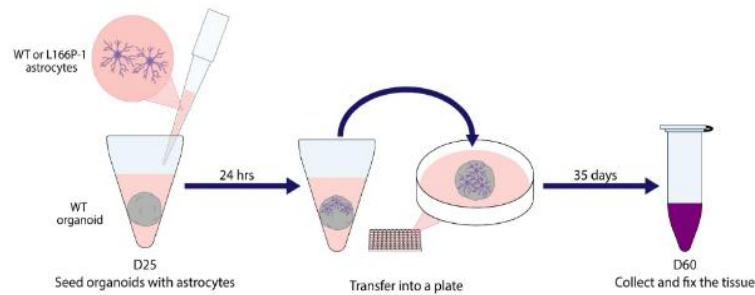


figura 2: gli astroцити sono stati trapiantati in organoidi all'interno di una piastra dal fondo a V. Dopo 24 ore, sono stati trasferiti in una piastra da 96 pozzetti, e mantenuti fino al giorno 60

2.4 SAGGIO SEAHORSE XF

Questo saggio permette di quantificare e confrontare la capacità glicolitica e il tasso di glicolisi in campioni cellulari. È stato utilizzato nello studio per verificare se l'aumento di AGEs fosse dovuto ad un aumento di espressione di qualche metabolita associato alla glicolisi o reattivo per la glicazione, oppure fosse dovuto alla perdita della funzione di DJ-1, in particolare della sua attività deglicasica.

Se in un primo campione cellulare aumenta il livello di AGEs rispetto ad un secondo, e parallelamente il tasso di glicolisi e la capacità glicolitica non varia tra i due, significa che nel primo campione è compromessa la funzione deglicasica.

2.5 SAGGIO QUANTITATIVO DQ RED BSA

Questo saggio permette di valutare l'attività proteolitica di una cellula. Viene utilizzata una sonda DQ-BSA che entra nel lume dei lisosomi e viene degradata dalle proteasi lisosomiali. Ciò comporta l'emissione di fluorescenza che può essere quantificata mediante appositi sensori. Il livello di fluorescenza misurato è quindi proporzionale all'attività di proteolisi lisosomiale della cellula.

2.6 ANALISI PROTEOMICA GLOBALE E FOSFOPROTEOMICA

Per questo tipo di analisi sono stati ottenuti diversi estratti cellulari utilizzando un buffer RIPA contenente gli inibitori delle proteasi e delle fosfatasi. Per ogni estratto sono stati prelevati campioni contenenti 40 µg di proteine, poi sottoposti a riduzione dei legami disolfuro. Dopo aver precipitato la componente proteica con una soluzione metanolo-cloroformio, i campioni sono stati digeriti con tripsina secondo un rapporto 100:1 proteina-proteasi. I peptidi così ottenuti sono stati etichettati mediante un TMT (*tandem mass tag*). Questo tag viene utilizzato per la quantificazione relativa delle proteine in analisi proteomiche, e consente di analizzare contemporaneamente anche più campioni. Tramite l'utilizzo di *high performance liquid chromatography* (HPLC) a fase inversa i campioni sono stati frazionati in sottocampioni. Dopo una fase di *desalting*, le frazioni ottenute sono state sottoposte ad analisi di spettrometria di massa.

La spettrometria di massa è una tecnica che permette di misurare con estrema precisione la massa di molecole. Le molecole analizzate, in questo caso proteine, devono essere ionizzate, per poi essere separate mediante degli analizzatori in base al rapporto massa/carica. Il risultato che si ottiene è uno spettro di massa nel quale ad ogni peptide viene attribuito un valore. Consultando *database* proteici, mediante opportuni algoritmi, si può correlare ad ogni valore un'identità. In questo modo, misurando la massa, è possibile capire quali frammenti proteici sono contenuti all'interno di un campione e in che quantità. Le principali qualità di questa tecnica sono l'accuratezza e la risoluzione. Ciò significa che il valore di massa misurato è molto vicino al valore reale, e che la spettrometria di massa è in grado di distinguere molecole aventi massa molto simile.

3. RUOLO DI DJ-1 IN ORGANOIDI UMANI DI MESENCEFALO

3.1 ORGANOIDI DJ-1 KO DIMOSTRANO DISFUNZIONI AUTOFAGICHE E ACCUMULO DI α -SINUCLEINA

I modelli prevalentemente utilizzati dal lavoro scientifico analizzato sono organoidi umani di mesencefalo, derivati da diverse linee cellulari. I hMIDOs di controllo sono stati ottenuti da una linea di cellule staminali umane pluripotenti indotte (hiPSC) BJSIPS proveniente da un individuo maschio sano. Da queste cellule è stata ricavata una linea isogenica con *knockout* DJ-1 in omozigosi o in eterozigosi mediante *CRISPR-Cas9 editing*. Il successo della mutazione è stato confermato tramite sequenziamento Sanger e *western blot*. È stata poi utilizzata una seconda linea cellulare hiPSC (KOLF 2.1J) sana e una sua linea isogenica avente la mutazione puntiforme DJ-1 L166P. Questa mutazione associata a PD determina la perdita di funzione della proteina e consiste nella sostituzione di una leucina con una prolina al residuo 166. A partire da queste cellule sono state ottenute due linee di cloni L166P-1 e L166P-2. L'importanza di avere linee isogeniche sta nel fatto che le eventuali alterazioni che si risconteranno tra mutato e controllo devono essere causate esclusivamente dalla mutazione e non da altre differenze nel *background* genetico.

Come già anticipato, a partire da queste linee cellulari sono stati generati diversi hMIDOs. La loro crescita è stata analizzata a diversi *time point* dall'inizio del differenziamento (40 giorni, 100 giorni e 200 giorni). In particolare, mediante tecniche di immunostochimica è stata verificata la presenza di proteine specifiche delle cellule del mesencefalo, di astrociti e di neuroni dopaminergici.

Dopo 40 giorni, gli hMIDOs DJ-1 L166P presentano livelli più bassi di NURR1, una proteina correlata al livello di maturazione del mesencefalo, suggerendo un ritardo dello sviluppo rispetto agli organoidi di controllo. Gli hMIDOs DJ-1 KO a questo *time point* invece non presentano significativi rallentamenti nello sviluppo. Dopo 100 giorni, la presenza della proteina GFAP evidenzia la crescita di astrociti, che aumenta fino ai 200 giorni. La presenza di MAP2, una proteina associata all'arborizzazione e quindi alla maturazione neuronale, conferma il corretto sviluppo degli organoidi. La presenza

di neuroni dopaminergici maturi è rilevabile grazie allo staining con GIRK2, e viene confermata dopo 200 giorni dall'inizio del differenziamento degli organoidi con la misurazione del livello di dopamina tramite spettrometria di massa. Nonostante i livelli di dopamina non varino significativamente tra hMIDOs DJ-1 KO e hMIDOs di controllo, è stata rilevata una significativa diminuzione di cellule positive a GIRK2 (un marcatore dei neuroni dopaminergici) nei primi: ciò dimostra che la mutazione di DJ-1 causa un decremento di neuroni dopaminergici negli organoidi.

Come già descritto, l'accumulo neuronale di forme aggregate e fosforilate di α -sinucleina contraddistingue diverse forme genetiche e sporadiche di PD. Per questo è stata misurata l'aggregazione di questa proteina nel tempo attraverso tecniche di *western blot* e *dot blot*. In hMIDOs DJ-1 KO si osserva un significativo aumento di α -sinucleina fosforilata monomerica rispetto ai controlli a partire dal giorno 200. Lo stesso risultato è stato ottenuto osservando i livelli di α -sinucleina in forma aggregata.

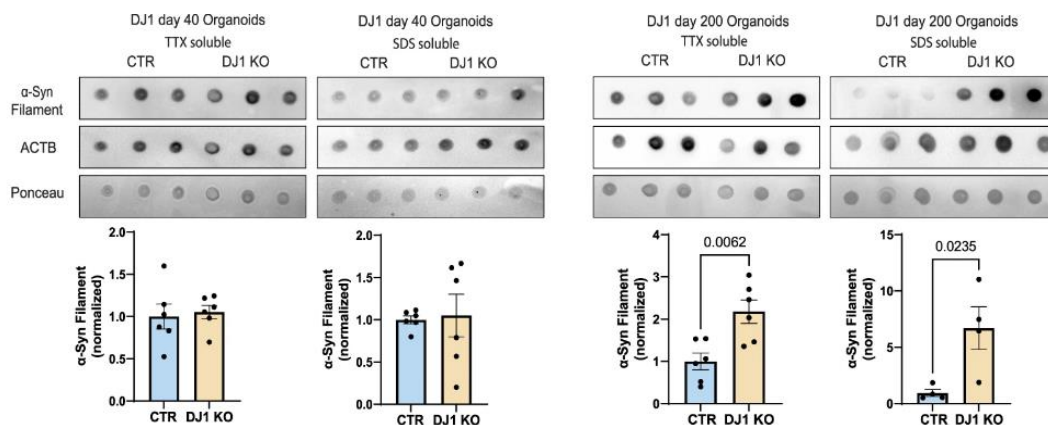


figura 3: confronto dei livelli di α -sinucleina aggregata solubile a TTX (detergente non ionico non denaturante) o a SDS (detergente ionico forte denaturante) tra hMIDOs DJ-1 KO e hMIDOs di controllo nei due diversi time point di 40 e 200 giorni

È noto che α -sinucleina monomerica o in forma aggregata indebitamente accumulata all'interno della cellula venga rimossa tramite processi lisosomiali di autofagia. In virtù dell'accumulo di α -sinucleina appena descritto, gli autori dell'articolo hanno voluto verificare se il KO di DJ-1 comprometta proprio queste funzioni. Per farlo sono stati

trattati degli organoidi di 100 giorni con bafilomicina A1 (BAF), un composto chimico che, impedendo l'acidificazione del lume lisosomiale, ne blocca l'attività. Utilizzando dei marcatori opportuni, si è verificato l'eventuale presenza di alterazioni nel livello di attività autofagica tra campioni BAF+ e campioni BAF-. Se in seguito all'esposizione a BAF l'attività autofagica non varia significativamente, vuol dire che già inizialmente era compromessa. Al contrario, se dopo l'esposizione a BAF l'attività autofagica diminuisce sensibilmente, significa che inizialmente avveniva in modo corretto.

Si sono perciò misurati tramite *western blot* i livelli di LC3-II in lisati di organoide: il suo livello basale in hMIDOs DJ-1 KO diminuisce rispetto a quello in hMIDOs di controllo. Inoltre, il flusso di LC3-II non varia significativamente tra hMIDOs DJ-1 KO trattati e non trattati con BAF. Ciò significa che l'autofagia in hMIDOs DJ-1 KO è compromessa. Non si sono invece evidenziate variazioni nell'accumulo di P62 tra hMIDOs DJ-1 KO trattati e non trattati con BAF, confermando ancora una volta la compromissione basale dell'attività autofagica in questi organoidi. I risultati finora descritti sono visibili in figura 4. Infine, è stata evidenziata una variazione significativa del livello di GBA tra hMIDOs DJ-1 KO e hMIDOs di controllo a partire dal giorno 200, dato che indica chiaramente una disfunzione lisosomiale.

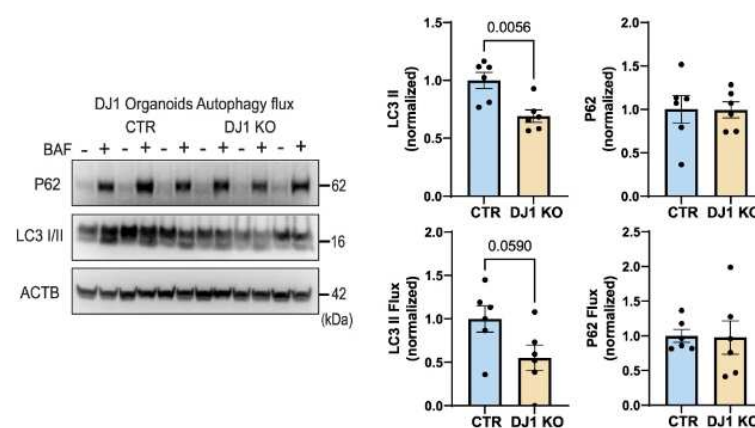


figura 4: confronto dei livelli di LC3-II e P62 con rispettivi flussi tra hMIDOs di controllo e hMIDOs DJ-1 KO

Questi risultati dimostrano come il *knockout* di DJ-1 comporti significative disfunzioni nei processi autofagici in modelli hMIDO, che a loro volta causano l'accumulo di α -sinucleina in forma monomerica fosforilata e in forma aggregata. Grazie agli esperimenti di immunostochimica inoltre vengono esposti gli effetti della mutazione al gene *PARK7* sulla maturazione del mesencefalo, tra i quali c'è una diminuzione del numero di neuroni dopaminergici.

3.2 ORGANOIDI DJ-1 KO ACCUMULANO PROTEINE DANNEGGIATE DA GLICAZIONE

In pazienti affetti da PD, gli AGEs e i rispettivi recettori (RAGEs) sono accumulati in grande quantità nella SN e nella corteccia cerebrale. Ciò è causato dai danni da stress ossidativo e porta a neurodegenerazione (22). È stato valutato l'accumulo di AGEs nei hMIDO, per indagare in che modo la perdita di funzione di DJ1 contribuisca a questo processo. Per farlo è stato misurato, mediante *dot blot*, il livello di *methylglyoxal-derived hydroimidazolone* (MGH), un prodotto iniziale del processo di glicazione. Come mostrato in figura 5 si osserva un notevole innalzamento di MGH in hMIDO DJ-1 KO di 100 e 200 giorni rispetto ai controlli. Non si notano invece alterazioni significative in hMIDO di 40 giorni e in iPSC, a dimostrazione del fatto che è necessario del tempo affinché questo fenotipo venga manifestato.

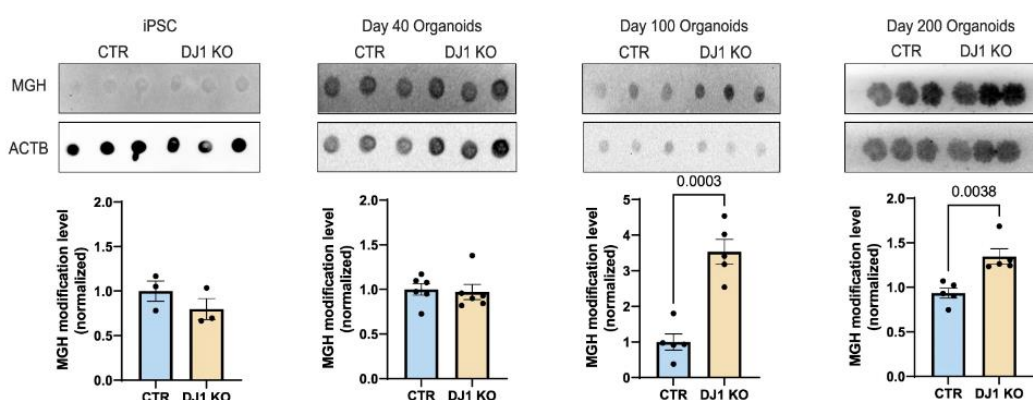


figura 5: dot plots sui livelli di MGH in diversi modelli DJ-1 KO, come cellule iPSC, hMIDO di 40, 100 e 200 giorni

Del tutto simili sono i risultati riguardanti i livelli di RAGEs, che sono affidabili *biomarker* della presenza di AGEs: in hMIDO di 200 giorni si osserva un netto aumento di queste molecole, così come parzialmente anche hMIDO di 40 giorni.

Grazie a *Seahorse XF assay* è stato determinato che l'aumento di MGH, che rispecchia l'incremento del livello di AGEs cellulare, sia da ricondurre ad una mancata attività riparatrice di DJ-1.

Un altro aspetto valutato riguardo all'effetto degli AGEs è stato il danno al DNA mediante l'analisi della presenza di fosforilazione negli istoni H2A.X. La fosforilazione di H2A.X è utilizzata come indicatore della frequenza con la quale gruppi carbonilici reattivi tossici tendono a reagire con residui di guanina, causando *double strand breaks* nelle catene di DNA(33). Infatti, i meccanismi di riparazione del DNA determinano la fosforilazione degli istoni. La presenza di P-H2A.X è quindi associata all'attività tossica dei prodotti di glicazione. In iPSCs DJ-1 KO il livello di P-H2A.X è più elevato rispetto ai controlli e, considerando che contemporaneamente non è stata misurata alcuna variazione di espressione basale di H2A.X, questo incremento può essere proprio ricondotto ad una maggior presenza di AGEs.

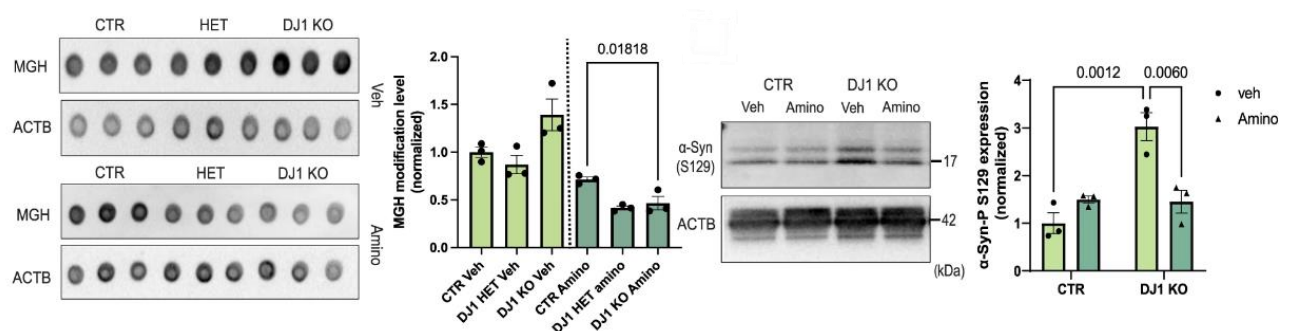


figura 6: confronto tra i livelli di MGH e P- α -syn in organoidi di controllo e organoidi DJ-1 KO. Sono stati utilizzati hMIDO di 100 giorni trattati con Amino per 40 giorni

Infine, per dimostrare la correlazione tra aumento degli AGEs e aumento dei livelli di α -sinucleina, gli organoidi sono stati trattati con aminoguanidina (Amino), uno

scavenger di gruppi carbonilici reattivi. In questo modo si può verificare se la rimozione del danno da glicazione migliori o recuperi i fenotipi associati a PD.

Il livello di MGH in hMIDOs DJ-1 KO trattati con Amino è notevolmente ridotto rispetto al livello osservato in organoidi non trattati, e così anche la quantità di α -sinucleina fosforilata, come mostrato in figura 6. Questi risultati confermano come la perdita di funzione di DJ-1 provochi un accumulo di AGEs, che a sua volta determina un fenotipo PD-associato come l'accumulo di α -sinucleina fosforilata.

4. RUOLO DI DJ-1 NEGLI ASTROCITI

4.1 LA PERDITA DI FUNZIONE DI DJ-1 INDUCE NEUROTOSSICITÀ

Finora sono stati osservati gli effetti generali della perdita di funzione di DJ-1 nell'intero organoide, nelle fasi successive dello studio le analisi si concentrano sul ruolo della proteina in una particolare classe di cellule gliali: gli astrociti. Essi costituiscono la principale popolazione cellulare a metabolismo glicolitico del sistema nervoso e sono perciò maggiormente esposti al rischio di danno da glicazione. Inoltre, queste cellule gliali sono cruciali per la corretta omeostasi neuronale, in quanto hanno il ruolo di degradare lipidi e proteine danneggiate tossiche, tra cui α -sinucleina(36,37).

Nelle colture di astrociti ottenute dagli organoidi è stato possibile allestire esperimenti grazie ai quali si è dimostrata la *non-cell-autonomous neurotoxicity* della perdita di funzione di DJ-1 mediata dagli astrociti stessi. Tale condizione si verifica nel momento in cui una prima cellula che presenta una mutazione induce una seconda cellula ad assumere un fenotipo alterato indipendentemente dal suo genotipo.

Sono stati trapiantati astrociti sani e della linea L166P in hMIDOs *wild type* di 25 giorni: gli organoidi sono stati fissati e sezionati dopo 60 giorni, momento nel quale gli astrociti endogeni non sono ancora cresciuti. L'inserimento di astrociti L166P ha portato ad una significativa riduzione di neuroni dopaminergici negli hMIDOs. Sono state inoltre allestite delle co-culture di NPCs assieme ad astrociti sia *wild type* che DJ-1-LOF. I risultati sono riassunti nella seguente tabella:

NPCs / ASTROCITI	EFFETTO
CNT/L166P	presenza di P- α -SYN
L166P/L166P	presenza di P- α -SYN
L166P/CNT	recupero della capacità proteolitica
CNT/L166P	perdita della capacità proteolitica

Questi risultati dimostrano come la capacità proteolitica della co-coltura venga compromessa qualora gli astrociti perdano la funzione di DJ-1, indipendentemente dal genotipo delle NPCs, causando l'accumulo di α -sinucleina. Gli astrociti L166P dimostrano inoltre alti livelli di GFAP, a dimostrazione del loro alto potenziale infiammatorio.

4.2 MECCANISMI CELLULARI COINVOLTI NELLA PERDITA DI FUNZIONE DI DJ-1

Per implementare i risultati finora ottenuti è stata effettuata una analisi proteomica globale e una analisi fosfoproteomica delle due linee cellulari L166P-1 e L166P-2 e dei loro rispettivi controlli KOLF 2.1J. Le due linee L166P hanno un'espressione proteica più simile tra loro rispetto alle linee di controllo. Tra le 8000 diverse proteine espresse identificate, 1192 lo sono differenzialmente. Ciò evidenzia un'importante alterazione del proteoma che include, ad esempio, l'incremento di α -sinucleina e di varie altre proteine ad alto rischio di aggregazione.

LINEA CELLULARE	DJ-1
KOLF 2.1J	attiva
L166P-1	perde funzione
L166P-2	perde funzione
BJSIPS	attiva
BJSIPS DJ-1 KO	knock out

Utilizzando la tecnica *Pathfinder* sono stati individuati i pathways cellulari maggiormente coinvolti dall'espressione differenziale delle proteine. La risposta infiammatoria risulta essere significativamente alterata, con un incremento dell'espressione di proteine associate a reattività e interleuchine pro-infiammatorie come IL32 e IL18. In particolare, la maggior espressione di IL18 è stata comprovata tramite tecniche di *immunostaining* sia in astrociti DJ-1 KO che L166P. Tutto ciò

dimostra che l'alterazione del proteoma porta ad un aumento dello stato infiammatorio degli astrociti, ad una maggiore reattività degli stessi e a rilascio di citochine.

Sono state poi riscontrate anche delle variazioni nel sistema ubiquitina/proteasoma (UPS): la proteolisi è chiaramente compromessa in astrociti DJ-1 L166P, dove si osserva un accumulo di α -sinucleina e di aggregati proteici in generale. In figura 7 vengono illustrati i risultati dell'analisi del livello di aggregati proteici mediante immunofluorescenza: la quantità di proteine aggregate in astrociti L166P 1 e 2 è maggiore rispetto a quella dei controlli. Trattando gli astrociti di controllo con MG-132, un inibitore del proteasoma, il livello di fluorescenza aumenta e si attesta su valori simili a quelli osservati nelle cellule L166P non trattate.

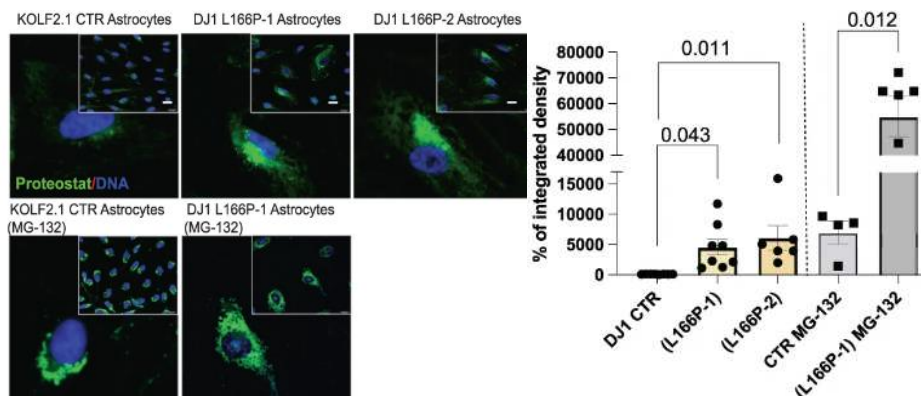


figura 7: analisi del livello di aggregati proteici in astrociti di controllo KOLF2.1, astrociti DJ1 L166P 1/2, astrociti KOLF2.1 trattati con MG-132 e astrociti DJ1 L166P 1/2 trattati con MG-132. Viene misurato il livello di fluorescenza di *proteostat*, un colorante specifico per proteine non correttamente ripiegate

Le analisi di fosfoproteomica forniscono informazioni riguardo siti differenzialmente fosforilati e diversa attività di specifiche chinasi. I risultati hanno dimostrato che su 10000 siti, 4709 presentano differenze di fosforilazione tra controlli e DJ-1 L166P. CDK e MAPKP8 sono le chinasi maggiormente coinvolte, con la loro attività, nell'alterazione della risposta infiammatoria e nella modulazione del citoscheletro.

4.3 LA PERDITA DI FUNZIONE DI DJ-1 IN ASTROCITI COMPROMETTE I LISOSOMI PORTANDO ALL'ACCUMULO DI α -SINUCLEINA

In modo simile a quanto descritto nel paragrafo 3.1 riguardo agli organoidi, la perdita di funzione di DJ-1 provoca un accumulo di aggregati proteici e disfunzioni autofagiche anche in astrociti. Sono stati svolti dei *western blot* su popolazioni di astrociti L166P e DJ-1 KO con rispettivi controlli per osservare i livelli e il flusso di LC3-II e P62, determinato grazie al trattamento con la BAF. I risultati sono illustrati nella figura 8.

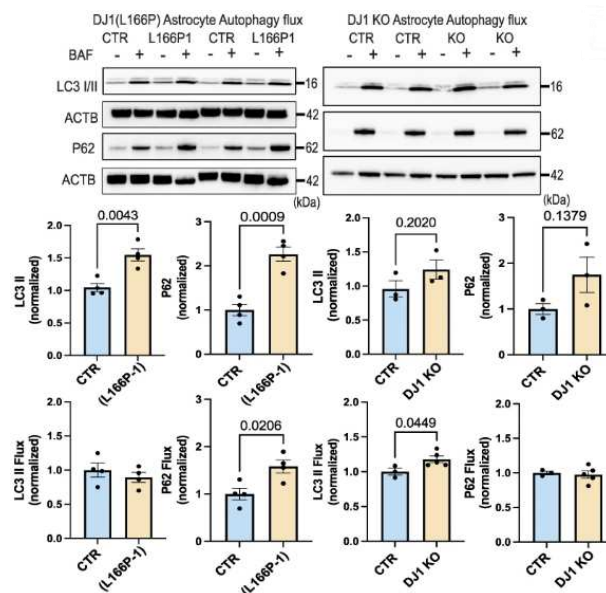


figura 8: analisi mediante western blot dei processi autofagici in astrociti DJ-1 L166P (a sinistra) e DJ-1 KO (a destra). I marcatori autofagici utilizzati sono LC3-II e P62

La popolazione di astrociti L166P ha un livello di LC3-II maggiore ma non incrementa nei campioni trattati con BAF, suggerendo che il flusso di autofagosomi non aumenta, mentre il loro numero sì, a causa di una maggior formazione o una minor degradazione. Parallelamente, anche P62 aumenta - confermando una diminuzione nella sua degradazione - così come il suo flusso, anche se in misura minore rispetto al controllo. La popolazione di astrociti DJ-1 KO ha risultati simili. Aumenta il livello di LC3-II, e anche per un 10% il suo flusso, suggerendo che vi sia un blocco del processo autofagico meno severo rispetto alla popolazione di astrociti L166P. Aumenta anche il livello di P62 ma non il suo flusso, confermando in modo coerente la disfunzione autofagica.

Con la perdita di funzione dei sistemi autofagici ci si aspetta un aumento dei livelli intracellulari di α -sinucleina: mediante tecniche di *western blot* e l'utilizzo degli inibitori BAF e MG132 sono stati ottenuti i risultati illustrati in figura 9.

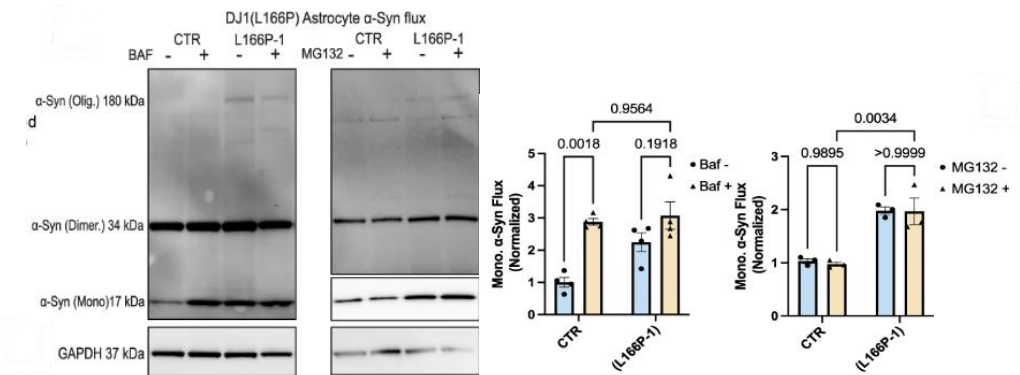


figura 9: flusso di α -sinucleina monomerica in astrociti DJ-1 L166P con o privi di trattamento BAF a sinistra e MG-132 a destra

In astrociti L166P-1 il flusso di α -sinucleina monomerica non varia significativamente in risposta al trattamento con BAF, contrariamente agli astrociti di controllo. Questo dato conferma ulteriormente che la mancata attività di DJ-1 causa un difetto nella degradazione degli aggregati proteici. Il sistema UPS non sembra contribuire alla degradazione di α -sinucleina in queste cellule, dal momento che i flussi non variano in risposta all'inibitore MG-132. il difetto degradativo è quindi prevalentemente a carico del processo autofagico.

Il trattamento di astrociti L166P e DJ-1 KO con Amino porta invece ad un abbassamento del livello di α -sinucleina complessivo, e a un evidente aumento della proteolisi lisosomiale (figura 10). Questo dato conferma che la ridotta capacità proteolitica dei lisosomi è dovuta almeno in parte al danno degli AGEs. Trattando infine gli astrociti mutati con MGO - un AGEs - si nota un significativo incremento del numero di nuclei apoptotici e del livello di caspasi, oltre che un abbassamento della già compromessa capacità proteolitica (figura 11).

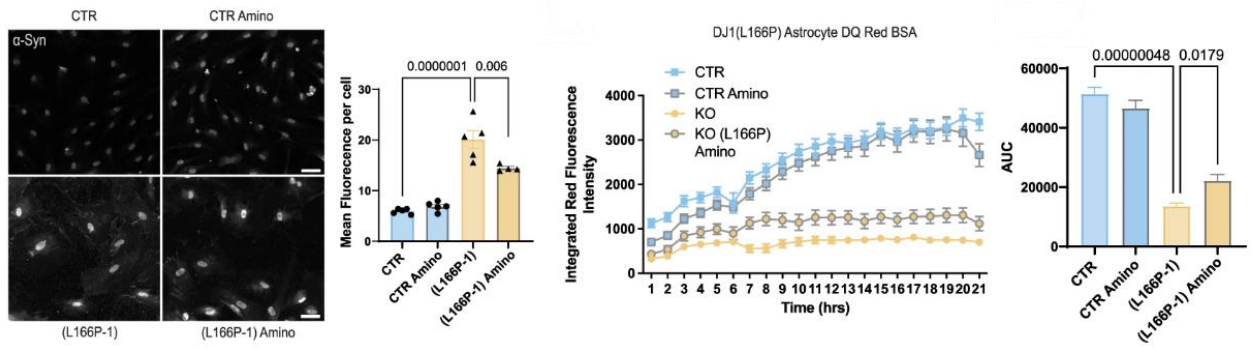


figura 10: il grafico a sinistra illustra i livelli di α -sinucleina, mentre quelli a destra rappresentano i livelli di attività proteolitica lisosomiale misurati attraverso la tecnica DQ Red BSA. Sono state analizzate diverse popolazioni di astroцити, alcune delle quali trattate con Amino.

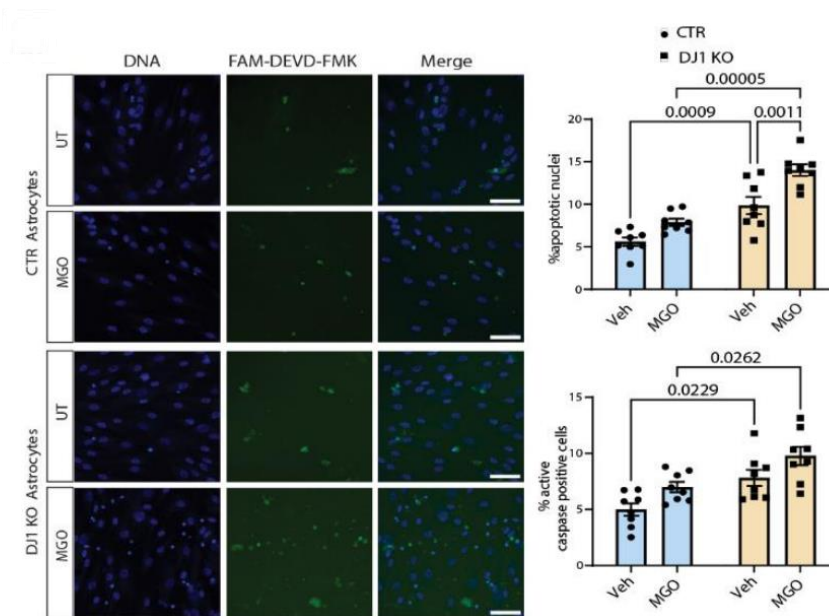


figura 11: confronto della percentuale di nuclei apoptotici e di cellule con caspasi attivate tra gruppi di astroцити di controllo e DJ-1 KO. Ogni popolazione è stata trattata anche con MGO per analizzare le variazioni delle percentuali

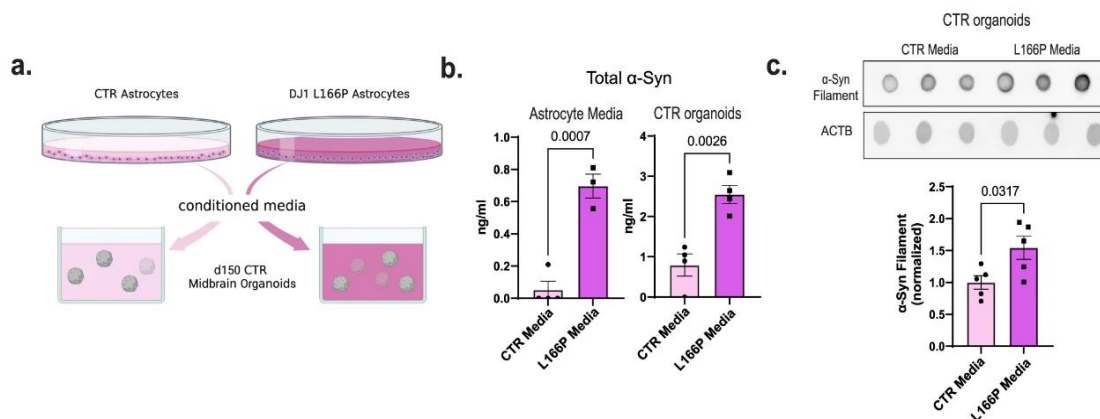


figura 12: (a) vengono trattati organoidi CNT con il terreno di coltura di astrociti DJ-1 L166P o di astrociti CNT (b) a confronto la quantità di α -sinucleina totale nel terreno di astrociti CNT e L166P, e in organoidi di CNT trattati con il media di coltura di astrociti CNT o DJ-1 L166P (c) la stessa analisi viene ripetuta per misurare l' α -sinucleina in forma aggregata

Come ultima analisi in questo studio è stato valutato il livello di tossicità dei fattori solubili rilasciati nel terreno di coltura degli astrociti privi della funzionalità di DJ-1. Come illustrato nella figura 12, il terreno di coltura di astrociti L166P presenta alti livelli di α -sinucleina, al contrario del terreno di coltura di astrociti di controllo dove la presenza è quasi nulla. Somministrando il terreno di coltura di astrociti L166P in organoidi di controllo si è osservato un significativo aumento sia del livello di α -sinucleina totale che della forma oligomerica. Ciò dimostra come questa mutazione in astrociti sia un fattore che induce l'accumulo di aggregati proteici tossici e una conseguente maggior morte cellulare neuronale.

5. CONCLUSIONI E DISCUSSIONE

La caratteristica patologica principale di PD consiste nella morte dei neuroni dopaminergici della *substantia nigra*. A livello cellulare, tra i fenotipi più comuni, si osservano neuroinfiammazione, stress ossidativo e accumulo di proteine non correttamente ripiegate, tra cui ad esempio α -sinucleina. Le cause di questa patologia possono essere sia ambientali che genetiche. In particolar modo sono stati identificati diversi geni la cui mutazione è causa di PD familiare. Si tratta di geni che portano a forme autosomiche dominanti di PD come *SNCA* (codificante α -sinucleina), e geni che portano invece a forme autosomiche recessive tra cui *PARK7* codificante DJ-1. È noto che questa proteina ha un ruolo associato allo stress ossidativo nella cellula. In campioni di corteccia cerebrale di pazienti soggetti a PD il livello della sua forma ossidata aumenta significativamente (32). Inoltre, è stato dimostrato che DJ-1 ha un'importante funzione enzimatica diretta contro la glicazione, e che una sua mutazione contribuisce a PD causando un lento accumulo di prodotti glicati dannosi. Infine, DJ-1 è coinvolta in meccanismi quali l'ossidazione della dopamina e l'autofagia. Nonostante queste conoscenze, i precisi meccanismi cellulari che associano l'attività di questa proteina alla patogenesi di PD non sono ancora del tutto chiari.

Essendo PD una patologia che causa la morte dei neuroni dopaminergici, storicamente gli studi di questa malattia si sono concentrati prevalentemente sulle cellule neuronali. Recentemente però l'attenzione si è spostata anche sul coinvolgimento delle cellule gliali, e sul ruolo che queste hanno nel processo di neurodegenerazione. Nel momento in cui queste cellule gliali non svolgono correttamente la loro attività di comunicazione con la popolazione di cellule neuronali e la funzione immunitaria, favoriscono lo sviluppo delle fasi precoci di PD e la morte dei neuroni dopaminergici(43,44). Si sono perciò svolti già diversi studi sugli astrociti: in modelli animali si è dimostrato come l'attività di DJ-1 in queste cellule gliali risulti protettiva contro lesioni chimicamente indotte a neuroni dopaminergici della SN(38,39). Al contrario, un KO al gene *PARK7* promuove una risposta infiammatoria e compromette i meccanismi per la riparazione delle lesioni(40). In campioni *post-mortem* di pazienti PD si è osservato un aumento di GFAP e di altre molecole coinvolte nella risposta infiammatoria degli astrociti(41,42).

I dati ottenuti dal lavoro scientifico analizzato in questa tesi hanno evidenziato quali meccanismi molecolari in particolare vengano compromessi dall'assenza di DJ-1 negli astrociti. Mediante *western blot* e analisi immunoistochimiche, è stato evidenziato uno stato di disfunzione lisosomiale, che porta all'accumulo di α -sinucleina aggregata in forme tossiche. Questa condizione danneggia il proteoma delle cellule del mesencefalo e porta gli astrociti ad attivare uno stato infiammatorio che aggrava la condizione patologica tipica del PD. La compromissione del sistema autofagico osservata in queste cellule gliali è, almeno in parte, dovuta all'incremento di AGEs intracellulari. Un'analisi proteomica e fosfoproteomica hanno permesso infine di descrivere ulteriori *pathways* alterati dalla mutazione del gene *PARK7*, come il sistema UPS e i meccanismi per il rimodellamento citoscheletrico.

Un punto di forza dell'articolo scientifico analizzato è sicuramente il modello utilizzato per svolgere i saggi e le analisi. Gli organoidi sono infatti in grado di rappresentare ottimamente le dinamiche fisiologiche e patologiche del mesencefalo umano. Questa caratteristica, insieme alla loro adattabilità e stabilità, li rendono ottimali per lo studio di PD e per testare eventuali nuove terapie. Un ulteriore punto di forza del lavoro è l'analisi proteomica globale e fosfoproteomica. Queste hanno permesso di identificare molti *pathways* significativamente coinvolti dalla perdita di funzione di DJ-1, oltre a quelli già analizzati con tecniche di *blotting* (incremento degli AGEs e disfunzione autofagica). Pertanto, queste analisi potranno essere utili anche in futuro per la caratterizzazione di diversi meccanismi molecolari regolati dall'attività di DJ-1. Ogni risultato ottenuto dall'analisi proteomica è stato validato da una seconda tecnica: l'alterazione citoscheletrica degli astrociti è stata confermata da immagini ottenute tramite *immunostaining*, così come l'aumento di citochine infiammatorie. La perdita di funzione del sistema di degradazione UPS è stata confermata da tecniche di immunofluorescenza che hanno evidenziato l'accumulo di aggregati proteici. Anche i risultati sulle disfunzioni autofagiche ottenuti tramite *western blot* sono stati confermati dal saggio DQ Red BSA, in grado di misurare la capacità proteolitica della cellula ¹.

Nonostante la consistenza delle analisi svolte nello studio analizzato e la qualità dei dati ottenuti, ci sono alcuni punti in cui i risultati non sono completamente convincenti. Ad esempio, per la misurazione degli AGEs è stato utilizzato un solo marcatore (MGH),

quando sarebbe stato opportuno utilizzarne anche un secondo. Non a caso nello studio è stata ammessa una discrepanza riguardo ai risultati sulle analisi del livello di RAGEs e di MGH in hMIDOs. Ciò può essere spiegato da due ipotesi: la prima è che i danni iniziali di glicazione sono sotto la soglia tecnica di detezione, la seconda che i danni iniziali da glicazione non sono necessariamente rappresentati da MGH. Inoltre, per recuperare il fenotipo indotto da accumulo di AGEs, gli autori utilizzano il trattamento con Amino. Questa sostanza è uno *scavenger* generico dei prodotti glicati, che ha dimostrato di poter risolvere in modo specifico i danni da glicazione in cellule che hanno perso la funzione di DJ-1. Non è detto tuttavia che Amino svolga esattamente la medesima attività di questa proteina. Sarebbe stato interessante osservare piuttosto quanto il ripristino della funzionalità di DJ-1 fosse in grado di risolvere l'accumulo di α -sinucleina nei modelli mutanti per il gene *PARK7*. Per fare ciò è possibile, ad esempio, indurre l'esprimere DJ-1 in una linea cellulare DJ-1 KO. Non sono state fatte inoltre analisi sugli effetti della sovraespressione di DJ-1, che avrebbero potuto arricchire la descrizione del suo ruolo cellulare.

Gli hMIDOs si prestano a nuovi studi che possono essere svolti in futuro. Riproducendo la diversità di classi cellulari presenti nel mesencefalo umano e le dinamiche di interazione che avvengono tra esse, gli organoidi rendono possibile analizzare ulteriori aspetti della patogenesi di PD. Su questi modelli è possibile, inoltre, effettuare *screening* di possibili sostanze terapeutiche, e quindi proseguire nella ricerca di nuove cure per PD. Sarebbe interessante, infine, utilizzare questi modelli per investigare sul ruolo di altre cellule gliali: sapendo ad esempio che una perdita di funzione di DJ-1 porta a neuroinfiammazione, potrebbe essere indagato in che modo le cellule della microglia contribuiscano allo sviluppo di PD. Si può concludere quindi che questo lavoro non solo abbia dimostrato nuove funzioni di DJ-1, ma abbia anche aperto diverse possibili strade affinché la ricerca scientifica produca nuova conoscenza e ci indirizzi alla scoperta di terapie efficaci contro la neurodegenerazione.

BIBLIOGRAFIA

1. Lucas JI, Marín I. A new evolutionary paradigm for the Parkinson disease gene DJ-1. *Mol Biol Evol.* febbraio 2007;24(2):551–61.
2. Wilson MA, Collins JL, Hod Y, Ringe D, Petsko GA. The 1.1-Å resolution crystal structure of DJ-1, the protein mutated in autosomal recessive early onset Parkinson's disease. *Proc Natl Acad Sci.* 5 agosto 2003;100(16):9256–61.
3. Nagakubo D, Taira T, Kitaura H, Ikeda M, Tamai K, Iguchi-Ariga SMM, et al. DJ-1, a Novel Oncogene Which Transforms Mouse NIH3T3 Cells in Cooperation with *ras*. *Biochem Biophys Res Commun.* 13 febbraio 1997;231(2):509–13.
4. Canet-Avilés RM, Wilson MA, Miller DW, Ahmad R, McLendon C, Bandyopadhyay S, et al. The Parkinson's disease protein DJ-1 is neuroprotective due to cysteine-sulfinic acid-driven mitochondrial localization. *Proc Natl Acad Sci.* 15 giugno 2004;101(24):9103–8.
5. Bonifati V, Rizzu P, Squitieri F, Krieger E, Vanacore N, van Swieten JC, et al. DJ-1 (PARK7), a novel gene for autosomalrecessive, early onset parkinsonism. *Neurol Sci.* 1 ottobre 2003;24(3):159–60.
6. Irrcher I, Aleyasin H, Seifert EL, Hewitt SJ, Chhabra S, Phillips M, et al. Loss of the Parkinson's disease-linked gene DJ-1 perturbs mitochondrial dynamics. *Hum Mol Genet.* 1 ottobre 2010;19(19):3734–46.
7. Thomas KJ, McCoy MK, Blackinton J, Beilina A, van der Brug M, Sandebring A, et al. DJ-1 acts in parallel to the PINK1/parkin pathway to control mitochondrial function and autophagy. *Hum Mol Genet.* 1 gennaio 2011;20(1):40–50.
8. Heo JY, Park JH, Kim SJ, Seo KS, Han JS, Lee SH, et al. DJ-1 Null Dopaminergic Neuronal Cells Exhibit Defects in Mitochondrial Function and Structure: Involvement of Mitochondrial Complex I Assembly. *PLOS ONE.* 5 marzo 2012;7(3):e32629.
9. Imberechts D, Kinnart I, Wauters F, Terbeek J, Manders L, Wierda K, et al. DJ-1 is an essential downstream mediator in PINK1/parkin-dependent mitophagy. *Brain.* 1 dicembre 2022;145(12):4368–84.
10. Hayashi T, Ishimori C, Takahashi-Niki K, Taira T, Kim Y chul, Maita H, et al. DJ-1 binds to mitochondrial complex I and maintains its activity. *Biochem Biophys Res Commun.* 18 dicembre 2009;390(3):667–72.
11. Zhang Y, Li XR, Zhao L, Duan GL, Xiao L, Chen HP. DJ-1 preserving mitochondrial complex I activity plays a critical role in resveratrol-mediated cardioprotection against hypoxia/reoxygenation-induced oxidative stress. *Biomed Pharmacother.* 1 febbraio 2018;98:545–52.
12. Taira T, Saito Y, Niki T, Iguchi-Ariga SMM, Takahashi K, Ariga H. DJ-1 has a role in antioxidative stress to prevent cell death. *EMBO Rep.* febbraio 2004;5(2):213–8.
13. Yokota T, Sugawara K, Ito K, Takahashi R, Ariga H, Mizusawa H. Down regulation of DJ-1 enhances cell death by oxidative stress, ER stress, and proteasome inhibition. *Biochem Biophys Res Commun.* 26 dicembre 2003;312(4):1342–8.
14. Mussakhmetov A, Shumilin IA, Nugmanova R, Shabalin IG, Baizhumanov T, Toibazar D, et al. A transient post-translational modification of active site cysteine alters binding properties of the parkinsonism protein DJ-1. *Biochem Biophys Res Commun.* 26 settembre 2018;504(1):328–33.
15. Wilson MA. The Role of Cysteine Oxidation in DJ-1 Function and Dysfunction. *Antioxid Redox Signal.* luglio 2011;15(1):111–22.

16. Xue Y, Wang AZ. DJ-1 plays a neuroprotective role in SH-SY5Y cells by modulating Nrf2 signaling in response to lidocaine-mediated oxidative stress and apoptosis. *Kaohsiung J Med Sci.* 2020;36(8):630–9.
17. Eleutherio ECA, Silva Magalhães RS, de Araújo Brasil A, Monteiro Neto JR, de Holanda Paranhos L. SOD1, more than just an antioxidant. *Arch Biochem Biophys.* 15 gennaio 2021;697:108701.
18. De Lazzari F, Agostini F, Doni D, Malacrida S, Zordan MA, Costantini P, et al. DJ-1 and SOD1 Act Independently in the Protection against Anoxia in *Drosophila melanogaster*. *Antioxidants.* 5 agosto 2022;11(8):1527.
19. González-Polo RA, Niso-Santano M, Morán JM, Ortiz-Ortiz MA, Bravo-San Pedro JM, Soler G, et al. Silencing DJ-1 reveals its contribution in paraquat-induced autophagy. *J Neurochem.* 2009;109(3):889–98.
20. Nash Y, Schumker E, Trudler D, Pinkas-Kramarski R, Frenkel D. DJ-1 deficiency impairs autophagy and reduces alpha-synuclein phagocytosis by microglia. *J Neurochem.* 2017;143(5):584–94.
21. Aryal B, Lee Y. Disease model organism for Parkinson disease: *Drosophila melanogaster*. *BMB Rep.* aprile 2019;52(4):250–8.
22. Stojkowska I, Wani WY, Zunke F, Belur NR, Pavlenko EA, Mwenda N, et al. Rescue of α -synuclein aggregation in Parkinson's patient neurons by synergistic enhancement of ER proteostasis and protein trafficking. *Neuron.* 2 febbraio 2022;110(3):436-451.e11.
23. Chaudhuri J, Bains Y, Guha S, Kahn A, Hall D, Bose N, et al. The Role of Advanced Glycation End Products in Aging and Metabolic Diseases: Bridging Association and Causality. *Cell Metab.* 4 settembre 2018;28(3):337–52.
24. Wollert T. Autophagy. *Curr Biol.* 22 luglio 2019;29(14):R671–7.
25. Mercer TJ, Gubas A, Tooze SA. A molecular perspective of mammalian autophagosome biogenesis. *J Biol Chem.* 13 aprile 2018;293(15):5386–95.
26. Hamasaki M, Furuta N, Matsuda A, Nezu A, Yamamoto A, Fujita N, et al. Autophagosomes form at ER-mitochondria contact sites. *Nature.* marzo 2013;495(7441):389–93.
27. Mizushima N. A brief history of autophagy from cell biology to physiology and disease. *Nat Cell Biol.* maggio 2018;20(5):521–7.
28. Mizushima N. The ATG conjugation systems in autophagy. *Curr Opin Cell Biol.* 1 aprile 2020;63:1–10.
29. Kumar AV, Mills J, Lapierre LR. Selective Autophagy Receptor p62/SQSTM1, a Pivotal Player in Stress and Aging. *Front Cell Dev Biol.* 14 febbraio 2022;10:793328.
30. Pang SYY, Lo RCN, Ho PWL, Liu HF, Chang EES, Leung CT, et al. LRRK2, GBA and their interaction in the regulation of autophagy: implications on therapeutics in Parkinson's disease. *Transl Neurodegener.* 31 gennaio 2022;11:5.
31. Burbulla LF, Song P, Mazzulli JR, Zampese E, Wong YC, Jeon S, et al. Dopamine oxidation mediates mitochondrial and lysosomal dysfunction in Parkinson's disease. *Science.* 22 settembre 2017;357(6357):1255–61.
32. Hasim S, Hussin NA, Alomar F, Bidasee KR, Nickerson KW, Wilson MA. A Glutathione-independent Glyoxalase of the DJ-1 Superfamily Plays an Important Role in Managing Metabolically Generated Methylglyoxal in *Candida albicans**. *J Biol Chem.* 1 gennaio 2014;289(3):1662–74.
33. Richarme G, Liu C, Mihoub M, Abdallah J, Leger T, Joly N, et al. Guanine glycation repair by DJ-1/Park7 and its bacterial homologs. *Science.* 14 luglio 2017;357(6347):208–11.

34. Andreeva A, Bekkhozhin Z, Omertassova N, Baizhumanov T, Yeltay G, Akhmetali M, et al. The apparent deglycase activity of DJ-1 results from the conversion of free methylglyoxal present in fast equilibrium with hemithioacetals and hemiaminals. *J Biol Chem.* 6 dicembre 2019;294(49):18863–72.
 35. Zhou W, Zhu M, Wilson MA, Petsko GA, Fink AL. The Oxidation State of DJ-1 Regulates its Chaperone Activity Toward α -Synuclein. *J Mol Biol.* 3 marzo 2006;356(4):1036–48.
 36. Tsunemi T, Ishiguro Y, Yoroisaka A, Valdez C, Miyamoto K, Ishikawa K, et al. Astrocytes Protect Human Dopaminergic Neurons from α -Synuclein Accumulation and Propagation. *J Neurosci.* 4 novembre 2020;40(45):8618–28.
 37. Kriks S, Shim JW, Piao J, Ganat YM, Wakeman DR, Xie Z, et al. Dopamine neurons derived from human ES cells efficiently engraft in animal models of Parkinson's disease. *Nature.* 6 novembre 2011;480(7378):547–51.
 38. Choi DJ, Eun JH, Kim BG, Jou I, Park SM, Joe EH. A Parkinson's disease gene, DJ-1, repairs brain injury through Sox9 stabilization and astrogliosis. *Glia.* 2018;66(2):445–58.
 39. De Miranda BR, Rocha EM, Bai Q, El Ayadi A, Hinkle D, Burton EA, et al. Astrocyte-specific DJ-1 overexpression protects against rotenone-induced neurotoxicity in a rat model of Parkinson's disease. *Neurobiol Dis.* 1 luglio 2018;115:101–14.
 40. Choi DJ, An J, Jou I, Park SM, Joe EH. A Parkinson's disease gene, DJ-1, regulates anti-inflammatory roles of astrocytes through prostaglandin D2 synthase expression. *Neurobiol Dis.* 1 luglio 2019;127:482–91.
 41. Song YJC, Halliday GM, Holton JL, Lashley T, O'Sullivan SS, McCann H, et al. Degeneration in Different Parkinsonian Syndromes Relates to Astrocyte Type and Astrocyte Protein Expression. *J Neuropathol Exp Neurol.* 1 ottobre 2009;68(10):1073–83.
 42. Tong J, Ang LC, Williams B, Furukawa Y, Fitzmaurice P, Guttman M, et al. Low levels of astroglial markers in Parkinson's disease: relationship to α -synuclein accumulation. *Neurobiol Dis.* 1 ottobre 2015;82:243–53.
 43. Kam TI, Hinkle JT, Dawson TM, Dawson VL. Microglia and astrocyte dysfunction in parkinson's disease. *Neurobiol Dis.* 1 ottobre 2020;144:105028.
 44. Wilson H, Dervenoulas G, Pagano G, Tyacke RJ, Polychronis S, Myers J, et al. Imidazoline 2 binding sites reflecting astroglia pathology in Parkinson's disease: an in vivo ^{11}C -BU99008 PET study. *Brain.* 1 ottobre 2019;142(10):3116–28.
-


APPENDICE






Disruption of lysosomal proteolysis in astrocytes facilitates midbrain organoid proteostasis failure in an early-onset Parkinson's disease model

Received: 5 October 2022

Accepted: 2 January 2024

Published online: 10 January 2024


 Check for updates

Gustavo Morrone Parfitt^{1,2,3,4,5,10}  , Elena Coccia^{1,2,3,4,5},
Camille Goldman^{1,2,3,4}, Kristen Whitney^{1,2,3,6,7}, Ricardo Reyes^{1,2,3,4},
Lily Sarrafha^{1,2,3,4}, Ki Hong Nam⁸, Soha Sohail^{1,2,3,4}, Drew R. Jones⁹,
John F. Crary^{1,3,6,7}, Alban Ordureau⁸, Joel Blanchard^{1,2,3,4,5,12}  &
Tim Ahfeldt^{1,2,3,4,11,12}  

Accumulation of advanced glycation end products (AGEs) on biopolymers accompanies cellular aging and drives poorly understood disease processes. Here, we studied how AGEs contribute to development of early onset Parkinson's Disease (PD) caused by loss-of-function of DJ1, a protein deglycase. In induced pluripotent stem cell (iPSC)-derived midbrain organoid models deficient for DJ1 activity, we find that lysosomal proteolysis is impaired, causing AGEs to accumulate, α -synuclein (α -syn) phosphorylation to increase, and proteins to aggregate. We demonstrated these processes are at least partly driven by astrocytes, as DJ1 loss reduces their capacity to provide metabolic support and triggers acquisition of a pro-inflammatory phenotype. Consistently, in co-cultures, we find that DJ1-expressing astrocytes are able to reverse the proteolysis deficits of DJ1 knockout midbrain neurons. In conclusion, astrocytes' capacity to clear toxic damaged proteins is critical to preserve neuronal function and their dysfunction contributes to the neurodegeneration observed in a DJ1 loss-of-function PD model.

Aging is the strongest risk factor for developing neurodegenerative diseases such as Alzheimer's Disease (AD) and Parkinson's Disease (PD)¹. Accordingly, investigating how biological mechanisms of aging are interconnected with the progression of neurodegenerative diseases is an active research area with significant therapeutic potential.

Recently, glycation, a process in which aldehyde metabolites and nucleophiles become attached to biopolymers through non-enzymatic reactions, has come into focus as a disease-driving mechanism. The accumulation of such advanced glycation end products (AGEs) on nucleotides, lipids, and proteins is known to damage

¹Nash Family Department of Neuroscience at Mount Sinai, New York, NY, USA. ²Ronald M. Loeb Center for Alzheimer's Disease at Mount Sinai, New York, NY, USA. ³Friedman Brain Institute at Mount Sinai, New York, NY, USA. ⁴Black Family Stem Cell Institute at Mount Sinai, New York, NY, USA. ⁵Aligning Science Across Parkinson's (ASAP) Collaborative Research Network, Chevy Chase, MD, USA. ⁶Department of Artificial Intelligence & Human Health, Icahn School of Medicine at Mount Sinai, New York, NY, USA. ⁷Department of Pathology, Molecular, and Cell-Based Medicine at Mount Sinai, New York, NY, USA. ⁸Cell Biology Program, Sloan Kettering Institute, Memorial Sloan Kettering Cancer Center, New York, NY, USA. ⁹Metabolomics Core Resource Laboratory, NYU Langone Health, New York, NY, USA. ¹⁰Present address: Department of Neuroscience, Genentech, Inc., South San Francisco, CA 94080, USA. ¹¹Present address: Recursion Pharmaceuticals, Salt Lake City, UT, USA. ¹²These authors jointly supervised this work: Joel Blanchard, Tim Ahfeldt.  e-mail: parfitt@gene.com; joel.blanchard@mssm.edu; tim.ahfeldt@recursionpharma.com

cell function and is a feature of normal aging². However, aberrant AGE accumulation has also been linked to multiple human pathologies, including aging-related neurodegenerative diseases such as PD. Both genetic and environmental factors contribute to the development of PD³, presenting challenges for identifying disease mechanisms that can be targeted therapeutically⁴. Recently, however, mutations in the α -synuclein gene (*SNCA*), the first identified causal mutations in PD³, were reported to impair proteome maintenance and cause protein aggregation⁵, highlighting protein quality control and autophagy as convergent disease-driving pathways in sporadic PD.

The protein DJ1, encoded by the *PARK7* gene, is causally linked to the development of early-onset PD by loss-of-function (LOF) mutations^{6,7}, but how the reduced function of DJ1 contributes to PD pathogenesis is not understood. Because a conserved cysteine residue in DJ1 is known to be frequently oxidized, it was initially suggested that DJ1 can sense the oxidative state of the cell^{8,9}. Indeed, highly oxidized sulfonated ($-\text{SO}_3^-$) forms of DJ1 are associated with its inactivation and are increased in the cortex of PD patients when compared to age-matched controls^{8,10}. More recently, several studies have established that DJ1 has glyoxalase activity and may function as a deglycating enzyme that protects DNA, proteins, or lipids from harmful glycation, although some controversy remains about DJ1 substrates and activity levels^{11–16}. In addition, studies using human-induced pluripotent stem cell (iPSC) models demonstrate that DJ1 impacts on oxidative stress pathways in neurons, particularly dopamine oxidation and autophagy pathways^{17,18}. Collectively, these findings suggest that decreased DJ1 activity resulting from ($-\text{SO}_3^-$) oxidation may contribute to PD pathogenesis.

Cell death in PD is restricted to discrete neuronal populations in a few brain areas, and more specifically to dopaminergic neurons (DNs) in the *substantia nigra* (SN), which has led to a neuro-centric view of PD pathology¹⁹. However, in recent years, genome-wide association studies have increasingly implicated glial-associated genes in PD²⁰. These findings are consistent with post-mortem analysis of PD cases, which often identifies astrocytes with a mild increase of GFAP in the SN, and accumulation of α -syn and PACRG in intracellular inclusions, unique features compared to the abundant astrogliosis observed in other neurodegenerative diseases^{21–23}. More recently, a scRNA-seq analysis identified a population of CD44/S100A6-high reactive astrocytes in the midbrain of PD patients²⁴. In addition, dysregulation of glial neuro-metabolic coupling and neuro-immune interactions were reported to have a crucial role in PD initiation and the death of the most vulnerable dopaminergic neurons^{25–29}. Together, these observations suggest that astrocytes have a causal role in PD pathogenesis.

Although DJ1 is abundantly expressed in the CNS, it's most highly expressed in astrocytes of the cortex and SN⁸. In animal models, DJ1 activity in astrocytes is protective against chemical-induced lesions to DN of the SN^{30,31}. Conversely, DJ1 knockout (KO) in mouse astrocytes leads to an exacerbated inflammatory response and impaired lesion repair³². Thus, although DJ1 has a well-established role as a protective protein in response to increased oxidative stress levels, more recently, its glyoxalase activity and role as a deglycating enzyme has been described. These findings propose that glycation stress is the core mechanism that underlies disease initiation and progression in DJ1 loss of function (LOF) early-onset PD.

The development of human midbrain brain organoids (hMIDOs) enabled the recapitulation of human midbrain tissue features such as mature TH-positive neurons and neuromelanin accumulation^{17,33}. hMIDOs recapitulate PD-related phenotypes in various PD mutations in long-term cultures such as reduction in TH⁺ dopaminergic and accumulation of α -syn oligomers and phosphorylated forms^{17,34}. Together with the scalability and stability of organoid models, hMIDOs make an ideal model for long-term studies and drug screening for PD pathology.

Here, we leverage a comprehensive panel of assays to investigate metabolic function in patient-derived human brain tissue and DJ1 LOF organoid iPSC models. We show that protein quality control pathways in astrocytes are defective in PD-associated DJ1 LOF. Accordingly, when DJ1 is missing or mutated, AGE accumulation and α -syn aggregation ultimately cause DN death. Our findings unravel the pathogenic role of astrocytes in aging and PD to uncover potential therapeutic strategies.

Results

DJ1 KO human midbrain organoids have PD-associated α -syn phenotypes

To study how DJ1 LOF impacts cellular processes in the absence of potential contributions from PD-associated genetics, we generated homozygous and heterozygous DJ1 knockout iPSC lines via CRISPR-mediated genome editing of BJSIPS iPSC line (originally derived from a healthy non-PD male). We confirmed the DJ1 KO via Sanger sequencing and Western blotting (Fig. S1A–B). In addition, we obtained a healthy male donor-derived hiPSC line KOLF 2.1J³⁵ and an isogenic line harboring the PD-associated DJ1 L166P LOF point mutation. We selected two clones which we hereafter refer to as L166P-1 and L166P-2.

To model the effects of DJ1 LOF on midbrain PD pathology, we generated human midbrain organoids (hMIDOs) using an established midbrain patterning protocol^{17,36} (Fig. 1a). Consistent with previous work, hMIDOs expressed midbrain markers FOXA2, LMX1A, and the mature midbrain marker NURR1, and generated TH⁺ neurons. At day 40, we found no differences in the expression of FOXA2, LMX1A, and NURR1 in DJ1 KO hMIDOs compared to control organoids (Fig. S1C). In contrast, we detected fewer NURR1-positive cells in organoids generated from the two DJ1 L166P clones (L166P-1 and L166P-2) (Fig. S1C). By day 100, astrocytes emerged, as reflected by GFAP expression, which became strongly increased by day 200 (Fig. 1b). In addition, the hMIDOs present extensive arborization when stained with a MAP2 marker at day 100 compared to day 40, indicating neuronal maturation. We confirmed the presence of mature dopaminergic neurons in organoids by day 100 by staining with GIRK2 and by measuring dopamine levels by mass spectrometry at day 200. We observed a significant reduction in the number of GIRK2 positive cells in the DJ1 KO (Fig. S1E), although dopamine levels did not differ between control and KO organoids (Fig. S1D).

The aggregation of the α -synuclein protein in the midbrain is a hallmark of PD³⁷. Consistent with this phenotype, we found that aged DJ1 KO hMIDOs contained significantly increased levels of monomeric phosphorylated α -syn at day 200 relative to isogenic control midbrain organoids (Fig. 1c). In contrast, we observed no significant difference in α -syn phosphorylation at day 40, suggesting that day 40 and 200 midbrain organoids represent early and late disease stages (Fig. 1c). Given that phosphorylation of α -synuclein at the S129 residue is correlated with α -syn turnover and accumulation in PD patients' brains³⁸, we next assessed α -synuclein aggregation via western blotting. In day 40 organoids, we did not observe significant differences in α -synuclein between DJ1 KO and controls (Fig. 1d). However, in TTX- and SDS-soluble fractions of day 200 DJ1 KO midbrain organoids, levels of aggregated α -syn had increased (Fig. 1d).

Lysosome pathways are essential to multiple forms of autophagy and are known to process α -syn monomers and aggregates. We consistently detect lysosomal function as a dysregulated pathway using proteomics analysis of human embryonic stem cells (hESCs) and day 35 hESC-derived hMIDOs lacking DJ1¹⁷. Here, we re-analyzed our proteomics dataset using pathway analysis to identify a wider range of cellular processes potentially related to lysosomal dysfunction (Fig. S1F). To investigate whether accumulation of α -synuclein aggregates in DJ1 KO hMIDOs was due to alterations in autophagy, we treated day 100 hMIDOs with bafilomycin A1 (BAF), which blocks lysosomal activity by inhibiting lysosome acidification. We then quantified levels of the autophagosome marker LC3 II, which is

generated through lipidation of LC3 I and essential for autophagosome formation. In BAF-treated samples, our analysis shows that LC3 II flux levels were not reduced significantly in DJ1 KO relative to CTR hMIDOs

although a significant reduction in the basal levels was observed (Fig. 1e). Similarly, accumulation of the autophagy substrate P62 was unchanged in BAF-treated KO hMIDOs (Fig. 1e). In addition, we

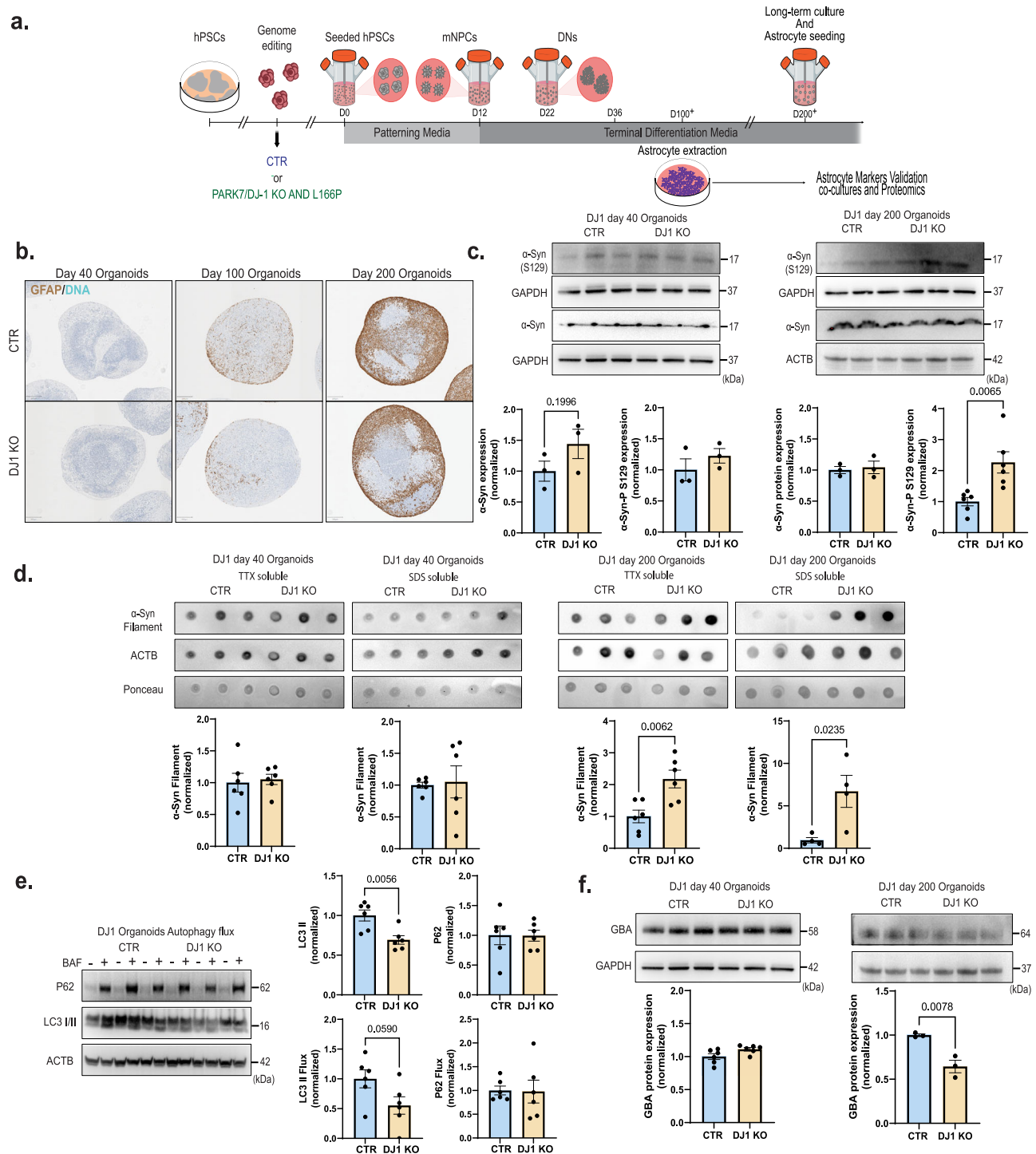


Fig. 1 | DJ1 KO human midbrain organoids α -syn and autophagy phenotypes.

a Micrography GFAP staining of CTR and DJ1 KO day 40, 100, and 200 midbrain organoids. **b** Midbrain differentiation and astrocytes extraction protocol schematic. **c** Immunoblots for α -syn, phospho- α -syn (S129) ($n = 3$, Two-tailed t -test), and corresponding loading controls actin (ACTB) and GAPDH for CTR and DJ1 KO day 40 (α -syn $n = 3$, phospho- α -syn (S129), $n = 3$) and day 200 midbrain organoids (α -syn $n = 3$; phospho- α -syn (S129), $n = 6$). **d** Dot blots for oligomeric α -syn and actin (ACTB)/Ponceau loading control for CTR and DJ1 KO day 40 TTX soluble ($n = 6$); SDS soluble fractions ($n = 6$) and day 200 TTX soluble ($n = 6$) and SDS soluble

fractions ($n = 3$) in midbrain organoids. **e** Immunoblots for LC3 I/II, P62, actin (ACTB) loading control in BAF - and + treated CTR and DJ1 KO day 100 midbrain organoids, graphs report LC3 I/II basal ($n = 6$), LC3 I/II flux ($n = 6$), P62 basal ($n = 6$), P62 flux ($n = 6$). **f** Immunoblots for GBA and ACTB/GAPDH loading control for CTR and DJ1 KO day 40 ($n = 6$) and day 200 ($n = 3$) midbrain organoids. All data are represented in mean \pm S.E.M, data points are individual well differentiation, and the p -value was reported on the graph highlighted comparison. For all the comparisons, a Two-tailed t -test was applied. Panels **c** and **f** share the same loading controls. All measurements were taken from distinct samples.

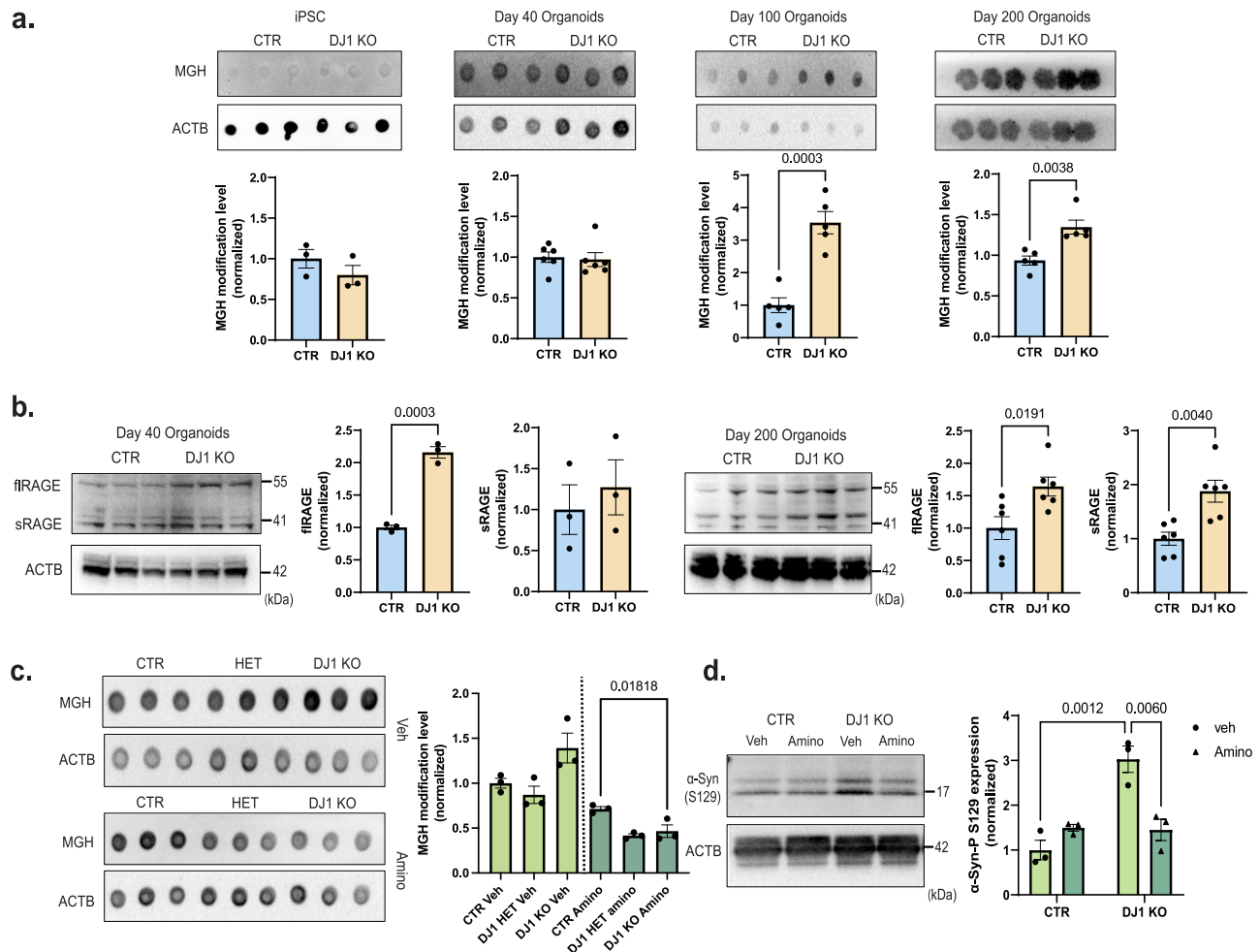


Fig. 2 | DJ1 KO midbrain organoids have increased protein glycation. **a** Dot blots for MGH protein modification and actin (ACTB)/Poncho loading control for CTR and DJ1 KO iPSCs ($n = 3$), day 40 ($n = 6$), 100 ($n = 5$), and 200 ($n = 5$) midbrain organoids (Two-tailed t -test was used for mean comparisons). **b** Immunoblots for fRAGE, for CTR and DJ1 KO day 40 ($n = 3$) and day 200 ($n = 6$) in midbrain organoids; actin (ACTB) was used as loading control (Two-tailed t -test was used for mean comparisons). **c** Dot blots for MGH protein modification and actin (ACTB) loading control in vehicle

(Veh) or aminoguanidine (Amino) treated CTR and DJ1 KO day 100 midbrain organoids ($n = 3$, Two-way ANOVA followed by Tukey's for the multiple comparisons test). **d** Immunoblots for phospho- α -syn (S129) and actin (ACTB) loading control in vehicle (Veh) or aminoguanidine (Amino) treated CTR and DJ1 KO day 200 midbrain organoids ($n = 3$, Two-way ANOVA followed by Bonferroni's for the multiple comparisons test). All data are represented in mean \pm S.E.M, data points are individual well differentiation, and the p -value was reported on the graph highlighted comparison. All measurements were taken from distinct samples.

observed depletion of the mature form of the lysosomal enzyme GBA on day 200 hMDOs but no alterations at day 40 (Fig. 1f), consistent with earlier reports in stem-cell-derived neuronal PD models^{39,40}. These results point to a failure of the autophagy system to compensate for the higher generation of aggregates in DJ1 KO hMDOs, overall causing the accumulation of oligomeric α -syn.

DJ1 KO midbrain organoids accumulate protein glycation damage

Oxidative damage, which compromises both proteome stability and cell viability^{41,42}, has been proposed to drive neurodegeneration through accumulation of advanced glycation end-products (AGEs)^{43,44}. In PD patients, AGEs and their corresponding RAGE receptors accumulate in the SN and cortex⁴⁵, potentially due to DJ1 dysfunction, given its reported role as a deglycase that maintains AGE homeostasis¹⁵. Here, we quantified Methylglyoxal-derived hydroimidazolone (MGH) levels, an initial advanced glycation modification, in iPSCs and human midbrain organoids via dot blots. Although MGH levels were equivalent in DJ1 KO and control in both iPSCs and day 40 midbrain organoids, MGH protein glycation accumulated significantly in day 100 and day 200 DJ1 KO hMDOs relative to controls (Fig. 2a).

RAGE expression is a sensitive biomarker for the presence of AGEs⁴⁶, therefore we were intrigued to observe a significant increased full-length and soluble RAGE protein at day 200 DJ1 KO, and partially in day 40 midbrain organoids (Fig. 2b). The increased levels of RAGE in day 40 organoids could indicate that early glycation damage is below levels of detection by MGH blotting or that non-MGH glycation damage is present. When we used the Seahorse XF assay, we found no change in the glycolysis rate (ECAR) or glycolytic capacity between the hMDO DJ1 KO and control midbrain organoids at day 40 or 100 (Fig. S2A). Similarly, mass spectrometry analysis did not reveal any differentially expressed metabolites correlated with increased reactive glycation or glycolysis (Fig. S2B). Collectively, these data suggest that the increase in AGEs observed in DJ1 KO midbrain organoids is likely a direct effect of the lack of DJ1's activity. However, mechanisms by which DJ1 caused the accumulation of AGEs could not be concluded from this set of experiments.

Next, we asked whether AGE accumulation in the midbrain contributes to classical PD phenotypes such as α -synuclein aggregation and lysosomal dysfunction. When we treated day 100 midbrain organoids for forty days with aminoguanidine (Amino), a scavenger of reactive carbonyl groups, we detected a significant reduction of MGH

glycated proteins in DJ1 KO midbrain organoids relative to amino-treated DJ1 CTR organoids (Fig. 2c). In parallel with reduced MGH, we also observed significantly decreased α -synuclein phosphorylation (S129) in Amino-treated DJ1 KO organoids (Fig. 2d). In contrast, there was no significant difference in α -synuclein phosphorylation in Amino-treated control organoids (Fig. 2d). The lack of alterations in DJ1 HETs was expected due to the autosomal recessive nature of the PD *PARK7* mutation. Because toxic reactive dicarbonyls that attack guanine residues in DNA can cause double-strand breaks¹⁵, we measured phospho-H2A.X (P-H2A.X) levels as an indirect readout for DNA damage response. We observed a consistent increase in the P-H2A.X levels in DJ1 KO iPSCs and hMIDO groups with no alterations in DJ1 HET iPSCs compared to CTR. However, no alteration in basal H2A.X levels was found among all the groups (Fig. S2C). Overall, these experiments suggest that AGEs may influence abundance and phosphorylation of α -synuclein.

Astrocyte DJ1 LOF causes non-cell-autonomous neuronal toxicity and impairs astrocytic metabolic support of midbrain neurons

Astrocytes are the principal glycolytic cell type in the brain and are, therefore, at a higher risk of acquiring glycation damage than neurons and other brain cell types. As astrocytes are essential for neuronal homeostasis and degradation of neuronal-derived damaged lipids and proteins such as α -syn^{28,47}, we next investigated astrocyte function in midbrain organoids. To this end, we developed a protocol for isolating astrocytes from mature midbrain organoids (day 100+) and maintaining them in 2D culture. Isolated astrocytes were immunoreactive for canonical astrocyte markers CD44, EAAT2, S100B, and GFAP (with no significant difference among genotypes) (Fig. S3A) and functionally responsive to ATP stimulation measured using the calcium sensor GCaMP7 (Fig. S3B). In addition, organoid-derived astrocytes were double positive for the midbrain makers *NURR1* and *FOXA2* and co-stained with CD49f and CD44 expression, confirming their midbrain identity⁴⁸ (Fig. S3C).

To investigate non-cell-autonomous effects of DJ1 loss of function mediated by astrocytes, we seeded day 25 hMIDO with mature L166P-1 or control astrocytes (Fig. 3a). We collected and fixed the tissue at day 60 when endogenous astrocytes were still not present in the organoids. We confirmed the graft efficiency with staining for the astrocyte marker CD44 (Fig. 3b). We found that adding L166P-1 astrocytes to WT midbrain organoids significantly reduced the number of TH-positive neurons (Fig. 3b). In addition, we co-cultured astrocytes with midbrain NPCs that, by day 50, expressed TH and featured mature neuronal morphology (Fig. 3a). Phospho- α -syn (S129) was present in DJ1 LOF astrocytes groups (L166P-1/L166P-1 and CTR/L166P-1) (Fig. 3c). When we analyzed total proteolysis capacity using DQ™ Red BSA, and found that the proteolysis capacity of the DJ1 LOF NPCs was significantly increased when co-cultured with CTR astrocytes (L166P-1/CTR) relative to L166P-1/L166P-1 groups (Fig. 3d). In addition, co-cultures of DJ1 LOF astrocytes with CTR NPCs (CTR/ L166P-1) proteolysis levels were disrupted when compared to the CTR/CTR group (Fig. 3d), suggesting that proteolytic clearance may be impaired in DJ1 LOF astrocytes. We also analyzed the protein levels of GFAP in astrocytes co-cultured with midbrain NPCs. When L166P-1 astrocytes were cultured with CTR or L166P-1 NPCs, a significant increase in GFAP levels was observed, demonstrating the inflammatory potential of DJ1 LOF in astrocytes (Fig. 3e).

To investigate these relationships in the human brain, we quantified cell-type expression of DJ1 in the midbrain of a cohort of PD patients (STable 1). We observed that GFAP-positive astrocytes were positive for ox-cys106 DJ1, which correlates with increased DJ1 activity (Fig. 3g). We also measured DJ1 activation levels by quantifying ox-cys106 DJ1 in the substantia nigra (SN) and midbrain. When compared to age-matched controls, PD patients had significantly increased levels

of ox-cys106 DJ1 in the SN and whole midbrain (Fig. 3f, STable 1). Collectively, this analysis suggests that DJ1 has a prominent neuro-protective role in astrocytes and that PD-associated DJ1 LOF variants contribute to neurodegeneration via astrocytes.

DJ1 LOF astrocytes have a pro-inflammatory phenotype and accumulate aggregated proteins

To identify pathways that contribute to non-cell-autonomous phenotypes mediated by DJ1 LOF astrocytes, we performed global TMT-proteomics and phospho-proteomics in astrocytes derived from 2 clones (L166P-1 and L166P-2) of KOLF 2.1J DJ1 L166P and their respective CTRs. The MS proteomic analysis identified ~8000 different proteins expressed in all samples. PCA analysis showed that the 2 DJ1 L166P clones clustered together and separated from the CTR. Therefore, we combined the two DJ1 L166P clones for the final analyses (Fig. S4A–B). In total, we identified 1192 differentially expressed proteins in the combined DJ1 L166P dataset (Fig. 4a, *P*-value of <0.01, logFC > 1.5 or <-1.5) indicating a significant proteome alteration that included upregulation of inflammatory/reactivity-related proteins such as ANXA3, FGB, AMIGO2, and SERPINE1 and pro-inflammatory interleukins IL32 and IL18 as the most highly differentially upregulated proteins in the DJ1 L166P astrocytes (Fig. 4a). When we probed our dataset for PD risk proteins, we found that α -synuclein and UCHL1 were increased, together with the mitochondrial redox balancing enzyme TXNRD2 (Fig. 4a).

To identify molecular pathways altered in DJ1 L166P astrocytes, we performed an enrichment analysis using the Pathfinder package, which considers protein-protein interactions. Among the top terms, we found the ubiquitin/proteasome system (UPS), cytoskeleton modification, and inflammatory responses (Fig. 4b, SData1). We then performed phospho-proteomics to identify differentially expressed phosphorylation sites and predict the most active kinases in DJ1 L166P astrocytes (Fig. S4D). We identified more than 10,000 different phosphorylated residues with 4709 differentially expressed based on this analysis. Using PhosR kinase activity prediction analysis, we identified the CDK isoforms and MAPK8 as the most likely phosphorylating proteins involved in regulating the cytoskeleton and inflammation, including the innate immune response regulator IRAK4 and other related proteins. In addition, when we plotted the CDK family with respect to differentially regulated phosphorylation sites, we observed auto-phosphorylation of CDK1 and increased phosphorylation in cytoskeletal proteins such as MAP4, MAP1B, MAPT, and septin9 (Fig. S4D). We also conducted pathway enrichment analysis for the CDK isoforms and MAPK8 using the top phosphorylation sites from our phosphoproteomics dataset. This analysis demonstrated their involvement in cytoskeleton remodeling (Fig. S4D).

Given that reactive astrocytes undergo key morphological change known as hypertrophy⁴⁹, we next performed immunostaining for the glial cell body marker CD44 and Hoechst 33342 to evaluate nuclear morphology (Fig. 4c). In the full DJ1 KO, we did not detect any alterations in the cell body area among the groups. However, the nuclear area was increased in DJ1 KO astrocytes, and both nuclear size and cell body area were increased in DJ1 L166P astrocytes (Fig. 4c). We also detected increased IL18 expression in both DJ1 KO and DJ1 L166P astrocytes, which is consistent with our proteomics analysis (Fig. 4d).

Our proteomics analysis of DJ1 L166P astrocytes identified alterations in proteolysis and an increase in α -synuclein. To relate these phenotypes with PD pathology, we performed multiple functional assays. In the presence of the ProteoStat dye (which binds and fluoresces in the presence of protein aggregates), fluorescence intensity was significantly increased in DJ1 L166P astrocytes, indicating an accumulation of protein aggregates (Fig. 4e). After treatment with the proteasome inhibitor MG-132, aggregation increased in both DJ1 L166P lines, and CTR astrocytes reached levels comparable to those found in UT L166P (Fig. 4e). DJ1 KO and DJ1 L166P astrocytes also expressed

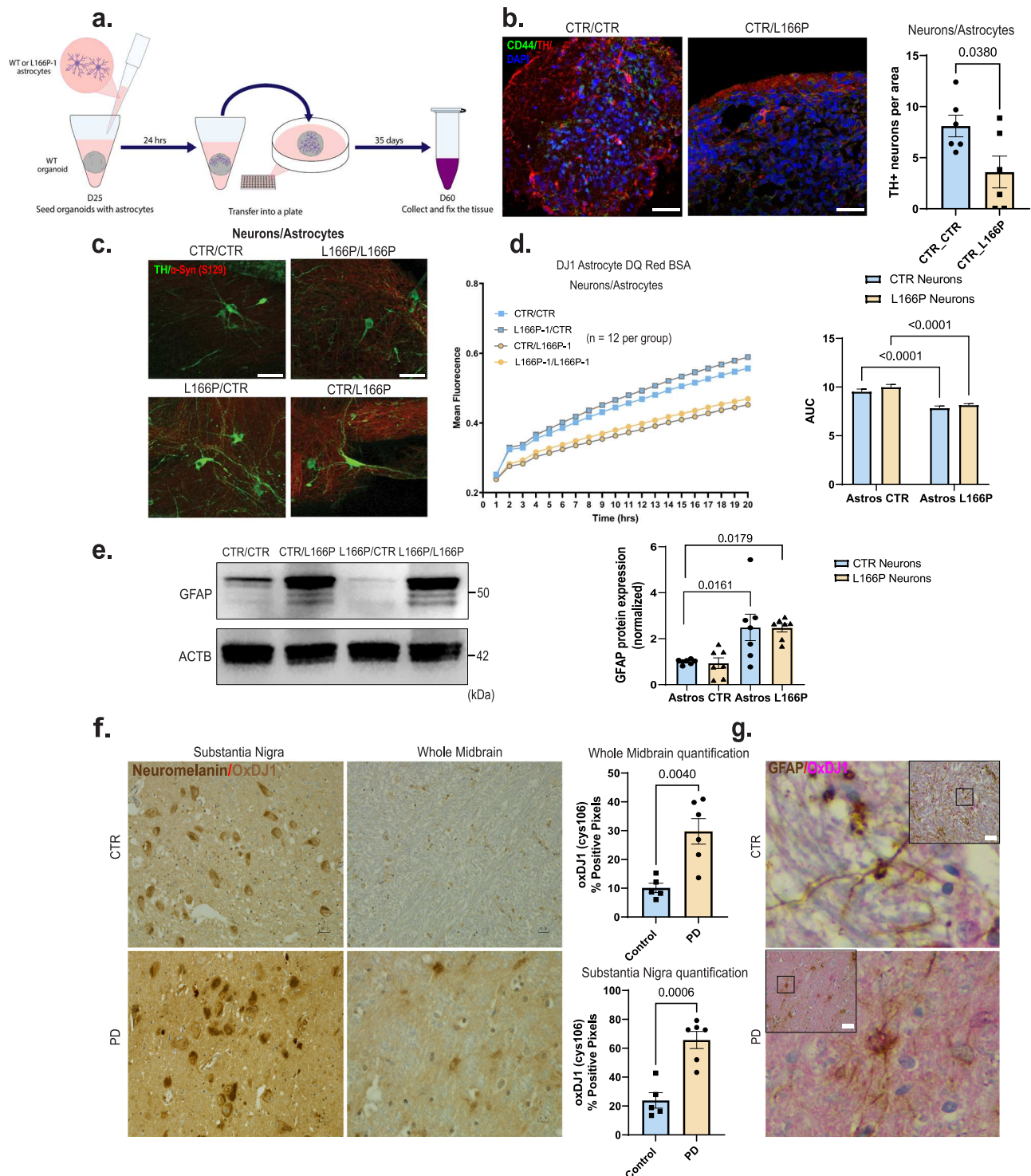
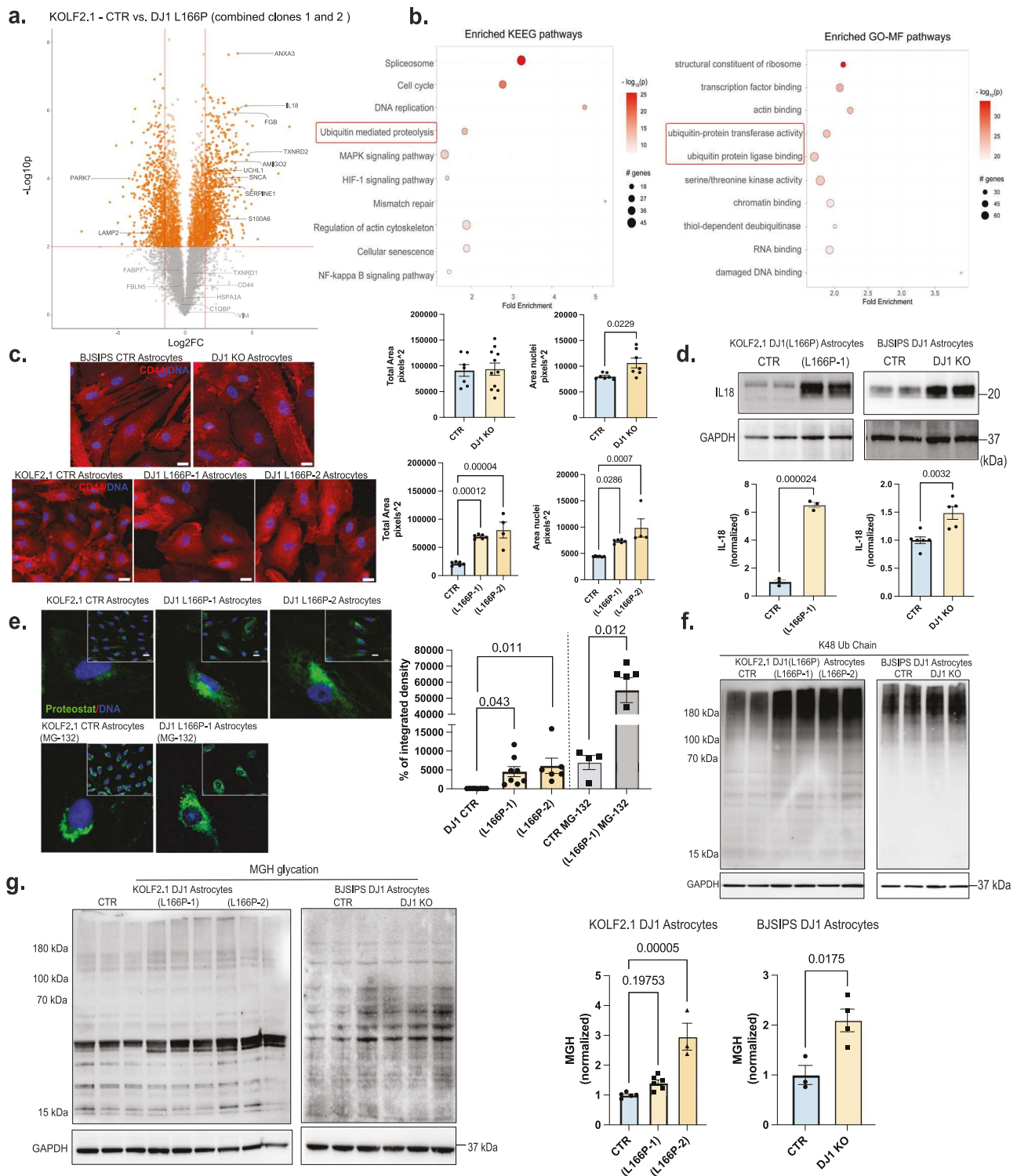


Fig. 3 | Astrocyte DJ1 LOF are reactive and produce toxicity in the midbrain.

a Astrocytes seeding procedure schematic. **b** Images of organoids seeded with astrocytes stained for TH (Red), CD44 (green), and DAPI and quantification of TH+ positive neurons per organoid area ($n = 6$, Two-tailed t -test was used for mean comparisons). **c** 40 \times images of day 50 NPC/Astrocyte co-cultures stained for TH (green), phospho- α -syn (S129) (Red). **d** DQ BSA proteolysis live imaging in mixed genetic neuron/astrocytes co-cultures ($n = 12$, Two-way ANOVA followed by Tukey's for the multiple comparisons test). **e** Western blot for GFAP and actin (ACTB) loading control for Neurons/Astrocytes co-cultures and quantification ($n = 7$, Two-

way ANOVA followed by Tukey's for the multiple comparisons test). **f** 40 \times micrograph of the *substantia nigra* and midbrain of PD patients and age-matched controls showing OxDJ1 staining in light brown. QuPath of OxDJ1 positive pixel quantification (CTR $n = 5$ and PD $n = 6$, Two-tailed t test was used for mean comparisons). **g** 40 \times micrograph GFAP positive midbrain astrocytes (brown) and OxDJ1 (red). All data are represented in mean \pm S.E.M. Scale bars, 50 μ m for (c), (f), and (g); 70 μ m for (b). Data points are individual well differentiation or individual patients, and the p -value was reported on the graph highlighted comparison. All measurements were taken from distinct samples.



higher levels of K48 ubiquitin chain proteins at high molecular weight, which is characteristic of protein aggregates (Fig. 4f). These observations indicate a higher UPS activity in DJ1 L166P combined with an inability to degrade protein aggregates. When we integrated the proteomics data with the aggregation risk scores (generated ZaggSC and TANGO⁵⁰) for each differential protein, we identified several proteins enriched in DJ1 L166P cells that were at increased risk for neurodegeneration-associated aggregation, such as APOA1, JADE1, and SERP1 (Fig. S4C). In addition, similar to DJ1 KO hMIDOs, DJ1 LOF in astrocytes also led to a significant increase in levels of MGH-glycated, with the exemption to clone L166P-1 (Fig. 4g). Altogether, these

analyses suggest that proteome instability leads to inflammation, reactivity, and cytokine release in astrocytes.

DJ1 loss of function impairs the lysosome, leading to accumulation of α -syn in astrocytes

Degradation of aggregated proteins, defined as autophagic flux (the rate of autophagic degradation) is upregulated in early stages of neurodegenerative diseases^{42,51}. We therefore sought to determine whether the accumulation of protein aggregates observed in DJ1 LOF astrocytes resulted from impaired autophagy or reduced ability to increase autophagy flux. When we analyzed autophagy flux in both DJ1

Fig. 4 | Pro-inflammatory and aggregated proteins are increased in DJ1 LOF astrocytes. **a** Volcano plot representation of TMT-labelled proteomics in KOLF 2.1J ($n = 3$) and DJ1 L166P-1 ($n = 3$) and L166P-2 ($n = 3$) midbrain astrocytes with selected proteins labeled (fold prioritization of LogFC vs. control of 1.5; Welch's t -test was used for the comparisons). **b** KEGG and FO-MF pathways enrichment analysis using pathfindR (p values were adjusted by the Bonferroni method) showing the selected top 10 terms. **c** 40 \times micrography of CD44 (red) and DAPI (blue) staining in BJ-SiPS CTR ($n = 7$) and KO ($n = 11$) astrocytes (Two-tailed t -test was used for mean comparisons) and KOLF 2.1J CTR ($n = 6$), DJ1 L166P-1 ($n = 6$), and L166P-2 ($n = 4$) astrocytes (One-way ANOVA followed by Tukey's for the multiple comparisons test). Quantification of cell total area based on CD44 staining and nuclear area based on DAPI staining. **d** IL18 in BJ-SiPS CTR ($n = 6$) and KO ($n = 5$) astrocytes and KOLF 2.1J CTR ($n = 3$), DJ1 L166P-1 ($n = 3$) astrocytes (Two-tailed t -test was used for mean

comparisons). **e** 40 \times micrography and quantification proteostat fluorescence levels in KOLF 2.1J CTR ($n = 8$), L166P-1 ($n = 8$) and L166P-2 ($n = 6$) (One-way ANOVA followed by Tukey's for the multiple comparisons test). 40 \times micrography and quantification proteostat fluorescence levels in KOLF 2.1J CTR + MG132 ($n = 4$), DJ1 L166P ($n = 60$) (Two-tailed t -test was used for mean comparisons). **f** Immunoblots for K48 ubiquitin chain and **g** MGH protein modification in KOLF 2.1J CTR ($n = 5$), L166P-1 ($n = 6$), and L166P-2 ($n = 3$) (One-way ANOVA followed by Tukey's for the multiple comparisons test). MGH protein modification in BJ-SiPS CTR ($n = 3$) and KO ($n = 4$) (Two-tailed t -test was used for mean comparisons). All data are represented in mean \pm S.E.M., data points are individual well differentiation, and the p -value was reported on the graph highlighted comparison. Proteomics data related to KN073-96 dataset. Scale bars, 20 μ m. All measurements were taken from distinct samples.

LOF astrocyte lines, we found that the levels of lipidated LC3 II increased significantly in L166P-1 BAF- treated group relative to untreated controls with no alteration in the DJ1 KO astrocytes (Fig. 5a). However, when we compared BAF- groups with their respective BAF+ treated controls, we observed a 10% significant increase in the DJ1 KO group in LC3 II flux levels, and no alteration in the L166P-1 group (Fig. 5a) suggesting that the formation of the autophagosome is not impaired in both DJ1 LOF lines. Next, we analyzed P62 flux to evaluate the ability of the autophagosome to degrade cargo. We found that levels of P62 increased significantly in the L166P-1 baseline and flux groups, and no alteration was found for DJ1 KO groups relative to untreated groups was observed (Fig. 5a).

Next, we assessed perinuclear localization of the lysosome, an essential feature for chaperone-mediated autophagy (CMA) activity and protein degradation⁵². In both DJ1 KO and DJ1 L166P astrocytes, we observed a decrease in perinuclear endo/lysosomes, as detected by LAMP1 and DAPI immunostaining, relative to the CTR group (Fig. 5b). Consistently, when we quantified proteolytic function using live imaging of DQTM Red BSA, which releases fluorescence upon proteolysis, we detected impaired proteolysis in both DJ1 KO and L166P astrocytes (Fig. 5c). Inhibition of the lysosome with BAF decreased fluorescence intensity, demonstrating that BSA proteolysis is largely performed by the lysosome (Fig. 5c). To deepen our understanding of the impaired lysosomal function, we next evaluated the presence of the early and late lysosomal damage markers GAL3 and K48 and the repair marker CHM4b⁵³. In the DJ1 L166P KO groups, percentages of LAMP1-positive puncta that were also positive for GAL3 and K48 were both increased, and we also observed an increase in K48 intensity per area relative to control (Fig. S5A). The percentage of LAMP1-positive puncta for the repair marker CHM4b also increased in the DJ1 L166P KO groups (Fig. S5A). Collectively, these data reveal that although the endo/lysosomal system in DJ1 L166P KO cells sustains more damage, it is still capable of triggering repair systems.

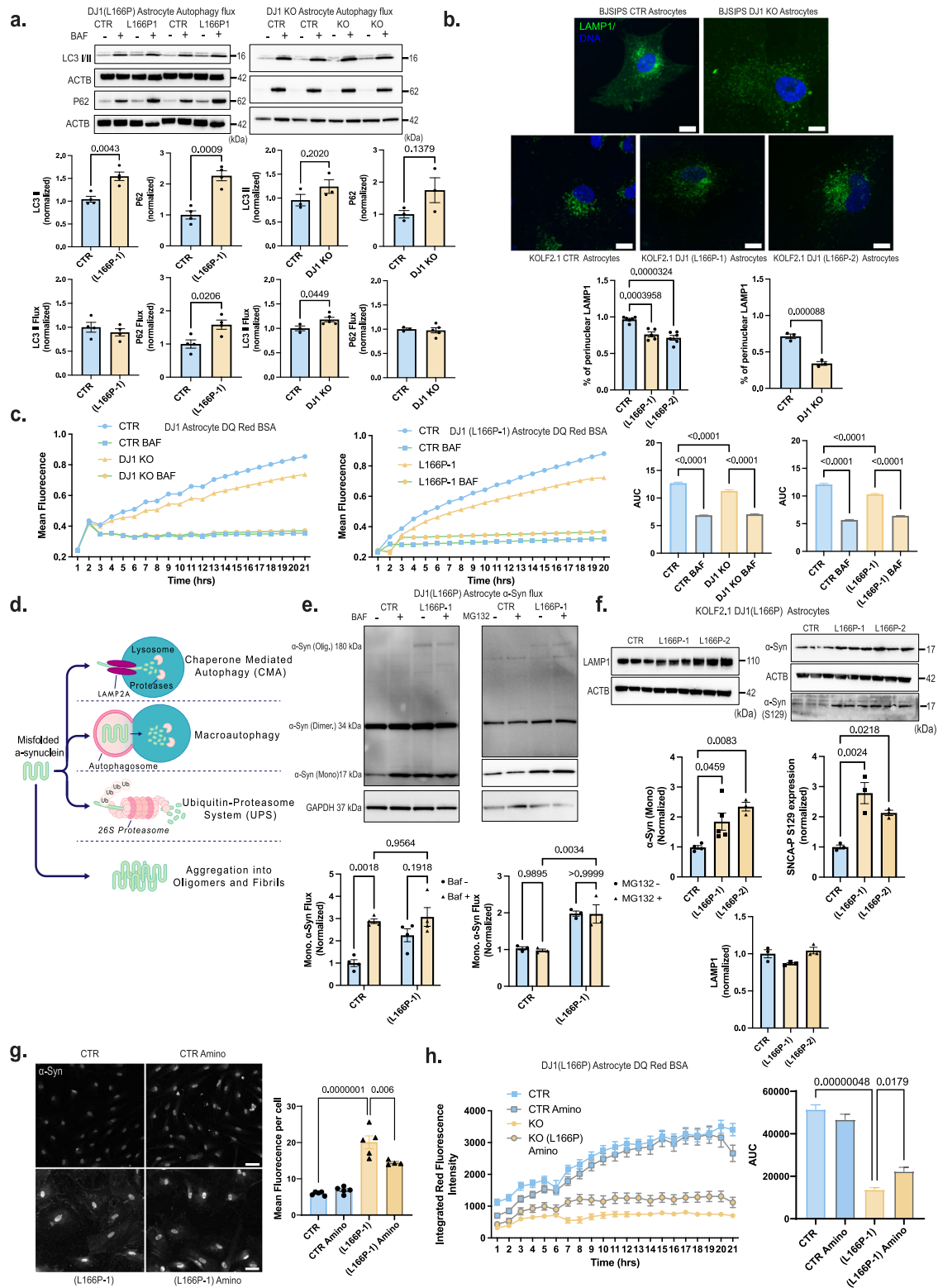
Toxic soluble and insoluble forms of α -syn are believed to accumulate in midbrain cells when degradation of aggregated forms through macro-autophagy fails to meet the demand of the elevated α -syn flux. α -Syn degradation is primarily performed by CMA and with the UPS as the preferred mechanism for aggregated forms (Fig. 5d). We analyzed the autophagy capacity to degrade monomeric α -syn, and found that monomeric α -syn in BAF-treated CTR increased, whereas the DJ1 L166P KO group had a decreased flux (Fig. 5e). Untreated DJ1 KO astrocytes also had significantly higher synuclein monomers than control astrocytes (Fig. 5e). In contrast, the amount of synuclein monomers in BAF-treated control astrocytes did not decrease, suggesting that DJ1 KO impairs the lysosomal clearance of synuclein monomers (Fig. 5e). Although the UPS is known to contribute to α -syn degradation⁵⁴, levels of α -syn did not significantly increase when control or DJ1 KO astrocytes were treated with the proteasomal inhibitor MG132, suggesting that proteasomal activity has minimal contribution to α -syn degradation in astrocytes (Fig. 5e). In addition, the monomeric unmodified and S129 phosphorylated forms of α -syn

increased in the DJ1 L166P lines compared to the CTR, while no alteration was observed in the endo/lysosome marker LAMP1 (Fig. 5f).

Based on our data thus far, we hypothesized that AGE damage is at least partly responsible for the reduced lysosomal proteolysis observed in DJ1 LOF astrocytes. When we treated astrocytes with the Methylglyoxal (MGO) scavenger Amino for 10 days, we noticed that lysosomal proteolysis was significantly improved in L166P KO astrocytes (Fig. 5h). Consistently, total α -syn levels were significantly reduced in treated relative to untreated KO L166P cells with no differences observed in treated controls (Fig. 5g). In addition, we tested if the treatment could reverse the DJ1 LOF DNA damage measured indirectly by phospho-H2AX. The levels of phospho-H2AX were significantly increased in L166P-1 astrocytes relative to CTR, with no differences between the L166P-1 vehicle versus L166P-1 Amino-treated astrocytes (Fig. S3F). This data indicates that Amino specifically relieves glycation damage in KO L166P cells. To evaluate glycation stress more specifically, we treated DJ1 KO astrocytes with the reactive dicarbonyl MGO, the main cause of glycation in live cells, and measured apoptotic nuclei and poly-caspase activation. Relative to untreated control cells, we detected significantly higher numbers of apoptotic nuclei and higher levels of poly-caspase in untreated DJ1 KO astrocytes (Fig. S3D). In addition, MGO treatment significantly increased the number of apoptotic nuclei in DJ1 KO, while no change in cell death hallmarks was observed in CTR astrocytes (Fig. S3D). When we examined proteolysis, we found decreased levels in DJ1 L166P astrocytes and that these levels were even further reduced by MGO treatment (Fig. S3E). To identify whether soluble factors released by the DJ1 LOF astrocytes could be toxic to neurons, we performed a conditioned media experiment on CTR organoids (Fig. 6a). We detected a significant increase in α -syn in both DJ1 L166P astrocytes media and media-treated CTR hMIDOs (Fig. 6b). We also detected a significant increase in soluble α -syn oligomers in hMIDOs treated with L166P astrocyte media, which indicates release of toxic soluble factors by L166P astrocytes (Fig. 6c). Altogether, our data show that DJ1 loss of function reduces lysosomal capacity, resulting in the accumulation of toxic forms of synuclein and increased neuronal cell death.

Discussion

Failed protein quality control and proteome damage are common features of several neurodegenerative diseases^{17,18,55}. Here, we show that DJ1 activity is essential to prevent accumulation of toxic damaged proteins in the midbrain. Although we did not detect alterations in soluble α -syn monomers as a consequence of DJ1 LOF, we detected an increase in soluble oligomers, indicative of dynamic relationships between α -syn oligomers and oligomerized or aggregated proteins that may be routed via different degradation processes. At a cellular level, our data show that DJ1 LOF or mutations hinder lysosomal processing of α -syn in astrocytes. Consequently, soluble α -syn oligomers aggregate into toxic forms, resulting in direct oxidative damage to the proteome of midbrain astrocytes and subsequent activation of astrocyte-derived inflammation signals that further aggravate



pathology. These data deepen and extend from the established view of astrocytes in PD inflammation.

Glycation is a form of oxidative protein damage commonly observed in diabetes, a risk factor for developing PD^{56,57}. We observed accumulation of MGH, an early form of glycation damage derived from MGO, in non-aggregated proteins in both hMDOs and isolated astrocytes. Nonetheless, non-aggregated glycated forms are thought to be degraded by the proteasome, and their build-up can trigger ER stress^{58,59}. In what way DJ1 protects from protein glycation damage is

still unclear. Early work proposed that DJ1 integrates with the glycation stress system through enzymatic function¹², participates in MGO degradation, or prevents permanent glycation damage by direct repair of early glycation products^{14,15}. In patient-derived iPSC neurons bearing DJ1 mutation glycation-related products were found elevated⁶⁰. However, DJ1 deficiency failed to enhance neuronal cell death when challenged with MGO⁶⁰. In the DJ1 KO organoids, we observe a progressive accumulation of glycated proteins starting at day 100. Glycolysis levels and MGO precursor metabolites were unaltered, which indicates a

Fig. 5 | DJ1 loss of function impairs proteostasis in astrocytes. **a** Immunoblots for P62, LC3 I/II, actin (ACTB) loading control in BAF - and + treated CTR and DJ1 KO in KOLF 2.1J and BJ-SIPS midbrain astrocytes. Immunoblots for LC3 I/II, P62, actin (ACTB) loading control in BAF - and + treated KOLF 2.1J CTR, DJ1 L166P-1 astrocytes, graphs report LC3 I/II basal ($n = 4$), LC3 I/II flux ($n = 4$), P62 basal ($n = 4$), P62 flux ($n = 4$). Immunoblots for LC3 I/II, P62, actin (ACTB) loading control in BAF - and + treated CTR and DJ1 KO astrocytes, graphs report LC3 I/II basal ($n = 3$), LC3 I/II flux (CTR, $n = 3$ and DJ1 KO, $n = 5$), P62 basal ($n = 3$), P62 flux (CTR, $n = 3$ and DJ1 KO, $n = 5$) (Two-tailed t -test was used for mean comparisons). **b** LAMP1 (green) and DAPI (blue) staining of astrocytes 40x images. Quantification of LAMP1 distribution staining in BJ-SIPS CTR ($n = 3$) and KO ($n = 3$) astrocytes (Two-tailed t -test was used for mean comparisons) and KOLF 2.1J CTR ($n = 6$), DJ1 L166P-1 ($n = 5$), and L166P-2 ($n = 7$) astrocytes (One-way ANOVA followed by Tukey's). **c** DQBSA proteolysis live imaging assay treated CTR and DJ1 L166P-1 KOLF 2.1J astrocytes (BAF -, $n = 40$, BAF + $n = 7$) or CTR and DJ1 KO BJ-SIPS (BAF -, $n = 39$, BAF + $n = 8$) treated with BAF- and

BAF + astrocytes (Two-way ANOVA followed by Tukey's). **d** Schematics showing α -syn degradation pathways. **e** Immunoblots for α -syn in BAF ($n = 4$) and MG132 ($n = 3$) - and + treated CTR and DJ1 L166P-1 KOLF 2.1J astrocytes (Two-way ANOVA followed by Tukey's). **f** Immunoblots for LAMP1 ($n = 3$), α -syn (CTR, $n = 3$; L166P-1, $n = 5$; and L166P-2, $n = 3$), phospho- α -syn (S129) ($n = 3$), and GAPDH loading control in and KOLF 2.1J CTR, L166P-1, and L166P-2 astrocytes (One-way ANOVA followed by Tukey's). **g** 40x images of total α -syn (gray) staining of astrocytes and quantification of vehicle (Veh) or aminoguanidine (Amino) treated astrocytes of CTR (CTR, $n = 5$; and CTR Amino, $n = 5$) or DJ1 L166P genotypes (L166P-1, $n = 5$; and L166P-1 Amino, $n = 4$) (Two-way ANOVA followed by Tukey's). **h** DQBSA proteolysis live imaging assay of vehicle (Veh) or aminoguanidine (Amino) treated astrocytes of CTR or DJ1 L166P-1 genotypes ($n = 24$, Two-way ANOVA followed by Tukey's). Scale bars, for b-15 μ m; g-40 μ m. All data are represented in mean \pm S.E.M., data points are individual well differentiation, and the p -value was reported on the graph highlighted comparison. All measurements were taken from distinct samples.

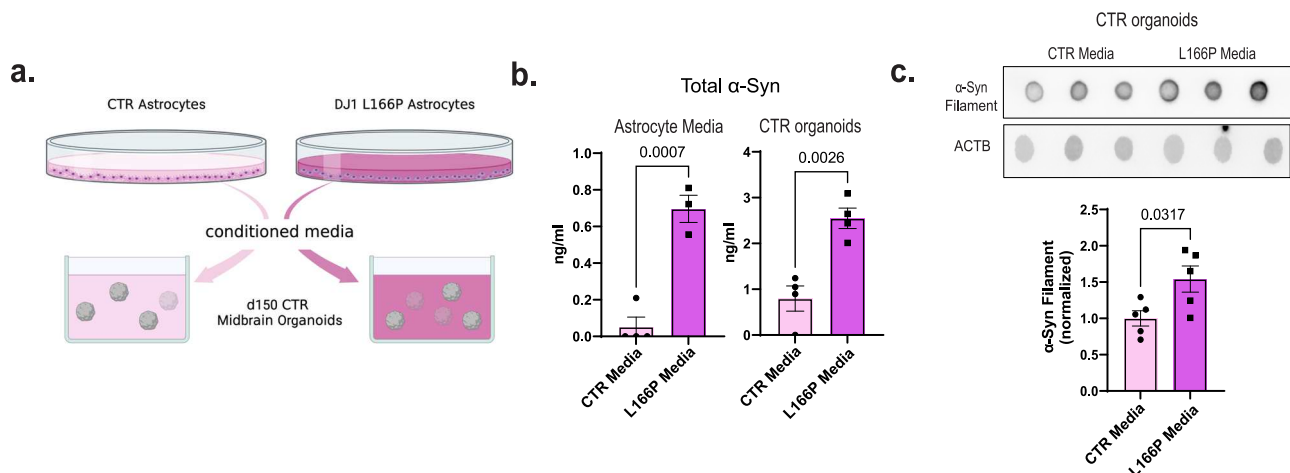


Fig. 6 | Astrocyte DJ1 loss of function conditioned media leads to α -syn increase in midbrain organoids. **a** Experimental design for conditioned media experiment, created with BioRender.com. **b** Competitive ELISA test for α -syn in media (CTR Media, $n = 3$; and L166P-1 Media, $n = 4$) and CTR organoid tissue ($n = 4$). **c** Dot plots for oligomeric α -syn and actin (ACTB) loading control for CTR ($n = 5$) and L166P

($n = 5$) astrocyte media treated midbrain organoids. All data are represented in mean \pm S.E.M., data points are individual well differentiation, and the p -value was reported on the graph highlighted comparison. All measurements were taken from distinct samples. For all the comparisons, a Two-tailed t -test was applied.

failure in MGO degradation or protein glycation repair. Conversely, presence of the carbonyl scavenger Amino decreased levels of MGH-modified proteins in both CTRs and DJ1 KO, validating its ability to prevent glycation stress, potentially by preventing the glycation stress-induced increase in α -syn phosphorylation. Altogether, these findings suggest that DJ1 participates in glycation metabolism, and DJ1 mutation contributes to PD by causing slow accumulation of deleterious glycation products.

In the absence of DJ1, levels of inflammatory cytokines IL18 and IL32 and downstream signal events such as IRAK4 phosphorylation were both increased. Consistently, the proteome analysis identified various upregulated proteins in DJ1 LOF astrocytes, such as ANXA3, S100A6, FGB, and SERPINE, while others, such as VIM and S100A10, were unchanged. These data reveal a unique astrocyte signature with relevance for PD-associated pathology, consistent with recent findings that reported glial cell activation upon scRNA-seq analysis of the human midbrain in PD patients²⁴. In a broad number of cells including astrocytes, cytoskeleton modification and changes in morphological features to sense, mobilize, or invade are the main characteristics of inflammation. Our proteome and phosphorylation pattern indicates an elevated modification of microtubule-associated proteins, which can explain the observed altered morphology of the DJ1 LOF astrocytes and the increase in nuclear size and cell body hypertrophy we observed in cells with the L166P mutation. We found differential

expression of MAP4, MAP1B, MAPT, and other proteins related to cytoskeleton modification. In addition, our prediction analysis identified the CDK kinase family, reported to phosphorylate cytoskeleton-associated proteins and other related proteins⁶¹, as the top active kinases predicted to phosphorylate the enriched residues.

Many PD genes participate in convergent pathways that are altered in the pathology⁶². Therefore, the finding that additional familial PD genes, such as *SNCA* and *UCHL1*, were upregulated in LOF DJ1 astrocytes was in line with these observations. We reported these changes in isolated astrocytes extracted from organoids, which points to the crucial contribution of astrocytes to specific PD phenotypes, such as α -syn accumulation. However, we cannot exclude a previously reported prion-like acquisition in which the spreading of α -syn throughout the hMIDOs causes damage⁶³.

In addition to lysosomal changes, we also identified UPS system alterations in our enrichment pathway analysis, consistent with the increase in aggregated protein inclusions and the sensitivity of the DJ1 mutation cell lines to proteasome inhibition. These relationships indicate the presence of ongoing protein damage that continuously needs to be repaired by the proteasome and lysosome systems. Although we only detected a mild alteration of autophagy in the L166P lines, α -syn oligomers were formed due to impaired lysosomal degradation of α -syn. Our observations indicate a varied phenotype depending on the type of mutation studied, with the DJ1 L166P

mutation harbouring the most deleterious phenotypes when compared to the DJ1 KO lines. The DJ1 L166P mutation generates an inactive truncated DJ1 protein which misfolds and therefore constantly needs to be degraded by the UPS system, which could further exacerbate the disease-associated phenotypes^{64,65}. In agreement, we found an increase in ATF6 in the DJ1 L166P cells, which increases activation due to the accumulation of misfolded products, leading to the induction of inflammatory gene networks⁶⁶.

Dysregulated networks common to early-onset and sporadic PD converge on proteostasis failure, causing accumulation of aggregated proteins^{17,18}. Based on our studies in the early-onset PD DJ1 model, we hypothesize that accumulation of glycosylated products, which overburden and damage protein degradation and repair systems, ultimately leads to proteostasis failure. In addition, due to their high non-aerobic glycolysis, astrocytes would be particularly vulnerable to this oxidative damage. In conclusion, we provide evidence that astrocytes dysfunction, glycation and widespread protein aggregation are fundamental phenotypes in familial DJ1-linked PD, pointing to strategies for developing more effective therapeutics.

Methods

Generation of isogenic knockout lines

Human iPSCs were cultured in standard conditions, and before nucleofection cells were pre-treated for 1 h. with 10 μ M Rhok inhibitor. 4×10^6 cells were dissociated using Accutase. Cells were pelleted and resuspended in 800 μ l PBS^{-/-} containing 5 μ g px330 CRISPR DNA each and transferred into nucleofection cuvettes. Nucleofection was performed using either the P3 Nucleofector kit from Amaxa and the standard and program CB-150 or the primary P4 Nucleofector kit from Amaxa and the standard and program hiPSC CA-137. The iPSC lines used for the generation of the TdTomato DJ1 WT, HET and KO were from the BJSIPS background and the guides as described in Ahfeldt¹⁷. The iPSC lines used for the generation of the DJ1 L166P point mutation were from KOLF 2.1J background³⁵ (Pantazis et al., 2021). DJ1 L166P clones 1 and 2 were used in this study. The parental cell lines were karyotyped prior to the beginning of the experiments. Genotyping PCR was used to identify clones with homozygous or compound heterozygous deletions leading to truncations and frameshift mutations. Clones for all lines containing deletions were identified by Sanger sequencing. No ethical oversight was necessary for this study.

Midbrain differentiation and organoid maintaining

hiPSCs were cultured in StemflexTM medium (ThermoFisher) at 37 °C, with 5% CO₂ in a humidified incubator, as previously described³⁶. For the organoid aggregation and differentiation, 125-ml disposable spinner flasks (Corning, VWR) were placed on a nine-position stir plate (Dura-Mag) at a speed of 65 rpm, as previously reported, starting with dissociated 40×10^6 hPSCs in Stemflex + Rhok inhibitor Y-27632 (4 μ M). Differentiation was initiated when spheres reached 300–500 μ m by dual-SMAD inhibition with SB431542 (R&D Systems, 10 μ M), LDNI93189 (Stemgent, 100 nM), B27-Vit A and N2 in DMEM-F12, to ensure the proper size range spheres were filtered using a set of 300 and 500 μ m filters (pluriSelect). Midbrain-specific patterning for midbrain NPCs organoids was the addition of CHIR99021 (Stemgent, 3 μ M), Purmorphamine (STEMCELL, 2 μ M), and SAG (Abcam, 1 μ M)⁴⁸. Post patterning Neural maturation medium was DMEM F12 medium containing N2, B27-VitA, 20 ng/mL GDNF (R&D Systems), 20 ng/mL BDNF (R&D Systems), 0.2 mM ascorbic acid (Sigma), 0.1 mM dibutyl cAMP (Biolong), 10 μ M DAPT (Cayman Chemical). For long-term maintenance (after day 35), the spheres were transferred to ultralow attachment plates (Corning, VWR) at five spheres per ml of media. The medium for long-term culture was DMEM F12 medium containing N2, B27-VitA, 10 ng/mL GDNF (R&D Systems), 10 ng/mL BDNF (R&D Systems), 0.2 mM ascorbic acid (Sigma).

Astrocyte differentiation and isolation

We derived astrocytic 2D cultures from large-scale 3D spin cultures, starting at day 90 using a protocol adapted from TCW et al.⁶⁷. This involved dissociation and serial passaging of midbrain organoids under conditions that favor astrocyte growth. Cells are grown in 125 ml flasks containing hundreds of individual organoids totaling more than 4×10^8 cells. Currently, the culture comprises various midbrain cell types including DNs, other neurons, progenitor cells, and astrocytic cell types. To isolate astrocytic progenitors, we gently triturated organoids in trypsin enzyme solution using a glass pipette to break up individual organoids into large chunks. After washing steps and pelleting of the organoids, we plated the suspension on 15 cm dishes coated with 0.1% gelatin. Cells are maintained in an astrocyte propagation medium (Astrocyte Medium, ScienCell #1801) for a week or until the first astrocytes are attached and start to divide. Cells were passaged to a maximum of P3. The maintaining and experimental media consisted of Advanced DMEM/F-12 (1 part, ThermoFisher 12634010), Neurobasal (1 part, ThermoFisher 21103049), B-27 Supplement, N-2 Supplement, MEM Non-Essential Amino Acids Solution (ThermoFisher 11140050), GlutaMAX (ThermoFisher 35050061), CNTF (10 ng/ml, PeproTech 450-13). For passaging, Astrocyte Medium was used on the first day and replaced by Astrocyte mature after 70% confluency was reached. For the conditioning media experiments, mature media was added to a confluent plate of astrocytes. After 3 days, the media was collected, filtered, and then added to day 150 hMIDOs.

Midbrain organoid astrocyte seeding and co-culture

For the co-culture experiments, midbrain NPCs of day 14 after differentiation and day 100 astrocytes were plated in a 96-well plate in a 5:1 proportion. They were maintained in a post patterning neural maturation medium for 2 weeks and then transferred to a long-term culture medium for the experimental procedures. For the seeding procedure, 12 organoids were seeded with 50k astrocytes each in a V bottom plate (Corning), and serum was added to the media to support the astrocyte seeding for 72 h. After 48 h, organoids were transferred to a 96-well plate, one organoid per well, and maintained until day 60.

Immunocytochemistry of fixed cells

Cells were fixed with 4% PFA for 20 min. Cells were blocked in 0.1% Triton X-100 (Sigma) in 5% horse serum/PBS, and then incubated in primary antibody (STable 2) (0.1% Triton X-100 in 5% horse serum/PBS) overnight at 4 °C. On the following day, cells were washed in PBS and incubated in species-specific fluorophore-conjugated Alexa fluor secondary antibodies and DAPI nuclear stain according to the manufacturer's protocol. The imaging was performed using the High content imager CX7 (Thermo Fisher) with a HCS Studio 4.0 software, and phenotyping and quantifications were performed using ImageJ v1.53 or CellProfiler v3 softwares. For the statistical analysis, the average of at least three fields of the well was counted as a N value.

Immunostaining and image analysis of sectioned spheres

Organoids were fixed with 4% PFA O/N and embedded in paraffin. Serial sections (4–6 μ m) of paraffin-preserved midbrain organoid sections were prepared using a Leica RM2255 microtome, sections were placed on charged slides and baked overnight at 70 °C. IHC was performed on Ventana Benchmark XT. Antigen retrieval with CCI (citric acid buffer) was performed for 1 h, followed by primary antibody incubation for 30 min (min.). A multimer secondary antibody was used for all samples. IHC sections were imaged using an Aperio VERSA 8 (Leica Biosystems, Wetzlar Germany) digital slide scanner and analyzed in QuPath (version 0.2.3, <https://QuPath.github.io/>).

Immunohistochemistry of human tissue

Cases and controls brain samples were derived from the Mount Sinai Neuropathology Brain Bank. Inclusion criteria were individuals with a neuropathological diagnosis of Parkinson's disease for cases and cognitively normal with no or only age-related neuropathological changes for controls. Formalin-fixed paraffin-embedded (FFPE) sections (5 μ m) were prepared from substantia nigra blocks, mounted on positively charged slides, and baked overnight at 70 °C. Immunohistochemistry (IHC) was performed on a Ventana Benchmark XT automatic staining platform (Roche Diagnostics, Indianapolis, IN) according to the manufacturer's protocol with reagents and antibodies acquired from the same lot. Antigen retrieval was done using CC1 buffer (Tris/Borate/EDTA buffer, pH 8.0–8.5, Roche Diagnostics) for 1 h followed by primary antibody incubation. All primary antibodies were diluted in antibody dilution buffer (ABD24, Roche Diagnostics). Primary antibodies were incubated for 36 min (mOXDJL, 1:400, Abcam) or 28 min (GFAP, 1:10, Ventana, 760-4345) followed by either 3,3'-diaminobenzidine (DAB) or alkaline phosphatase for visualization. For slides that were double-labeled, both DAB and alkaline phosphatase were used for visualization. All slides were counterstained with hematoxylin and coverslipped.

Digital histopathologic analysis

For unbiased digital quantitative assessment, slides were imaged using an Aperio VERSA 8 (Leica Biosystems, Wetzlar Germany) digital slide scanner. Whole tissue sections and the substantia nigra were manually neuroanatomically segmented on whole slide images (WSI) and analyzed in QuPath (version 0.2.3, <https://QuPath.github.io/>). All analysis was batch-processed using a custom positive pixel-based analysis workflow that measured the percentage of positive pixels detected using a positive pixel classifier based on thresholded values for DAB intensity. All quantitative values were normalized to the area.

Live-cell imaging to access lysosome function

Astrocyte monocultures or midbrain neuronal/astrocyte co-cultures were plated in the 96-well plates. Cells were incubated with DQTM Red BSA, which emits red fluorescence upon proteolysis, for 30 min, washed 3 times with PBS, and kept in maintaining media throughout the assay. Bafilomycin A2 (100 nM, Sigma-Aldrich B1793) was added to specific wells to confirm the lysosomal nature of the proteolysis. Aminoguanidine (30 μ M) was used for the reversal experiments. The plates were incubated for image acquisition in Incucyte[®] Live-Cell Analysis System for 21 h and images were analyzed in the Incucyte[®] software v2020C.

Calcium Imaging in astrocytes

For GCaMP8s imaging, plated astrocytes in 2 cm gelatin-coated plates were placed on a Nikon Eclipse TE2000-U microscope, with a 10 \times objective. GCaMP8s was excited using a 480 nm (Mic-LED-480A, Prizmatix), an HQ480/40 \times excitation filter, a Q50SLP dichroic mirror, and an HQ535/50 m emission filter (Semrock). Fluorescence was projected onto an sCMOS Zyla chamber camera (VSC-01910, Andor), and sampled at a rate of 4.7 fps with a frame exposure of 200 ms at 160 \times 120 pixels (4 \times 4 binning). The light source and sCMOS camera were controlled with the Nikon Elements software (NIS-Elements AR 5.20.01). The astrocytes were continuously perfused during fluorescence recording with ACSF with the following composition (in mM): NaCl 125, KCl 5, D-Glucose 10, HEPES-Na 10, CaCl₂ 3.1, MgCl₂ 1.3. The ATP treatment (100 μ M) was controlled by a ValveBank8 II (AutoMate Scientific Inc.). ROI segmentation of GCaMP8s, raw fluorescence extraction, and background correction was performed with Nikon Elements software. $\Delta F/F$ was calculated using R-studio (R version 4.0.3).

Western blotting and dot blot

Cell culture lysates were generated using RIPA buffer (Thermo Scientific), 1 or 2% SDS lysis buffer (10 mM Tris, 150 mM NaCl, 1 mM EDTA)

containing protease inhibitor cocktail (Thermo Scientific), and phosphatase inhibitor cocktail (Thermo Scientific). Protein concentration was estimated using the BCA assay (Pierce). For Western blot analysis, 20–40 μ g total protein was denatured under reducing conditions in 4 \times Laemmli Sample Buffer (Bio-Rad) by heating for 10 min at 70 °C before loading onto a 10% Criterion TGX Precast gel (Bio-Rad), then transferred to a PVDF membrane (0.22 μ m; Bio-Rad) using the iBlot 2 dry blotting system (Invitrogen). Membranes were blocked for 1 h at RT in 5% w/v non-fat milk (Santa Cruz) in TBS containing 0.1% v/v Tween-20 (Fisher Scientific; TBS-T). Membranes were then incubated in the indicated primary antibody (in 5% milk/TBS-T) overnight at 4 °C, washed 4 times in TBS-T, incubated in species-specific HRP-conjugated secondary antibody (in 5% milk/TBS-T) for 1 h at RT, and then washed 4 times in TBS-T. Membranes were subsequently developed with ECL Western blotting substrate (Pierce). Membranes were then washed once in TBS-T and stripped in stripping buffer (25 mM Glycine HCl, pH 2.0, and 1% w/v SDS) with vigorous shaking to remove primary and secondary antibodies, washed three times in TBS-T, and blocked for 1 h (in 5% milk/TBS-T) at RT before probing with the next primary antibody. Dot blots were performed in the same way as western blots but without the gel separation step. The primary antibodies are listed in STable 2.

Proteomics—cell lysis and protein digestion

At the indicated times, cells were washed twice with ice-cold PBS and snap-frozen. Cell pellets were lysed with in-house RIPA buffer (50 mM HEPES, 150 mM NaCl, 1% sodium deoxycholate, 1% NP-40, 0.1% SDS, 2.5 mM MgCl₂, 10 mM sodium glycerophosphate, 10 mM sodium biphosphate) containing in-house protease and phosphatase inhibitor cocktail, to produce whole-cell extracts. Whole-cell extracts were sonicated and clarified by centrifugation (16,000 $\times g$ for 10 min at 4 °C) and protein concentrations were determined by the Bradford assay. Protein extracts (40 μ g) were subjected to disulfide bond reduction with 5 mM TCEP (room temperature, 10 min) and alkylation with 25 mM chloroacetamide (room temperature, 20 min). Methanol–chloroform precipitation was performed before protease digestion. In brief, four parts of neat methanol were added to each sample and vortexed, one part of chloroform was then added to the sample and vortexed, and finally three parts of water were added to the sample and vortexed. The sample was centrifuged at 8000 rpm for 5 min at room temperature and subsequently washed twice with 100% methanol. Samples were resuspended in 100 mM EPPS pH8.5 containing 0.1% RapiGest and digested at 37 °C for 16 h with trypsin at a 100:1 protein-to-protease ratio.

Proteomics—Tandem Mass Tag labeling

Tandem Mass Tag (TMT and TMTpro) labeling of samples was carried out as followed. For total proteome analysis (40 μ g of digested peptides), 8 μ L of a 10 μ g/ μ L stock of TMT reagent was added to samples, along with acetonitrile to achieve a final acetonitrile concentration of approximately 30% (v/v). Following incubation at RT for 1 h, the labeling efficiency of a small aliquot was tested for each set, and the reaction was then quenched with hydroxylamine to a final concentration of 0.5% (v/v) for 15 min. The TMT-labeled samples were pooled together at a 1:1 ratio. The total proteome sample was vacuum centrifuged to near dryness and subjected to C18 solid-phase extraction (SPE) (50 mg, Sep-Pak, Waters).

Proteomics—off-line basic pH reversed-phase (BPRP) fractionation

Dried TMT-labeled sample was resuspended in 100 μ L of 10 mM NH₄HCO₃ pH 8.0 and fractionated using basic pH reverse phase HPLC. Briefly, samples were offline fractionated over a 90 min run, into 96 fractions by high pH reverse-phase HPLC (Agilent LC1260) through an aeris peptide xb-c18 column (Phenomenex; 250 mm \times 3.6 mm), with

mobile phase A containing 5% acetonitrile and 10 mM NH₄HCO₃ in LC-MS grade H₂O, and mobile phase B containing 90% acetonitrile and 10 mM NH₄HCO₃ in LC-MS grade H₂O (both pH 8.0). The 96 resulting fractions were then pooled in a non-continuous manner into 24 fractions used for subsequent mass spectrometry analysis. Fractions were vacuum centrifuged to near dryness. Each consolidated fraction was desalted via Stage Tip, dried again via vacuum centrifugation, and reconstituted in 5% acetonitrile, and 1% formic acid for LC-MS/MS processing. For Phospho-peptides, dried peptides were fractionated according to the manufacturer's instructions using High pH reversed-phase peptide fractionation kit (Thermo Fisher Scientific) for the final 6 fractions and subjected to C18 StageTip desalting prior to MS analysis.

Proteomics–Fe²⁺-NTA phosphopeptide enrichment

Phosphopeptides were enriched using Pierce High-Select Fe²⁺-NTA phosphopeptide enrichment kit (Thermo Fisher Scientific, A32992) following the provided protocol. In brief, dried peptides were enriched for phosphopeptides and eluted into a tube containing 25 μ L 10% formic acid (FA) to neutralize the pH of the elution buffer and dried down. The unbound peptides (flowthrough) and washes were combined, dried up, and subjected to basic pH reversed-phase fractionation (see method section) and used for the total proteome analysis (non-phosphorylated peptides).

Proteomics–Total proteomics analysis

Mass spectrometry data were collected using an Orbitrap Eclipse Tribrid mass spectrometer (Thermo Fisher Scientific, San Jose, CA) coupled to an UltiMate 3000 RSLCnano system liquid chromatography (LC) pump (Thermo Fisher Scientific). Peptides were separated on a 100 μ m inner diameter microcapillary column packed in-house with -30 cm of HALO Peptide ES-C18 resin (2.7 μ m, 160 \AA , Advanced Materials Technology, Wilmington, DE) with a gradient consisting of 5–23% (0–75 min), 23–40% (75–110 min) (ACN, 0.1% FA) over a 120 min run at -500 nL/min. For analysis, we loaded 3/10 of each fraction onto the column. Each analysis used TMT-MS₂ based quantification, combined with the FAIMS Pro Interface (using previously optimized 3 CV parameters for TMT multiplexed samples⁶⁸). The scan sequence began with an MS₁ spectrum (Orbitrap analysis; resolution 120,000 at 200 Th; mass range 400–1500 m/z ; automatic gain control (AGC) target 4×10^5 ; maximum injection time 50 ms). Precursors for MS₂ analysis with desired charge state (z : 2–6) were selected using a cycle type of 1.25 s/CV method (FAIMS CV = -40/-60/-80). MS₂ analysis consisted of high energy collision-induced dissociation (HCD) and was analyzed using the Orbitrap (resolution 50,000 at 200 Th; NCE 38; AGC 2×10^5 ; isolation window 0.5 Th; maximum injection time 172 ms). Monoisotopic peak assignment was used, precursor fit filter was used (80% fit) and previously interrogated precursors were excluded using a dynamic window (150 $s \pm 10$ ppm). For TMTpro analysis, a similar setup was used with the following modifications. Each analysis used Multi-Notch MS₃-based TMT quantification⁶⁹, combined with a newly implemented Real-Time Search analysis software^{70,71}. MS₂ analysis consisted of collision-induced dissociation (quadrupole ion trap analysis; Rapid scan rate; AGC 1.0×10^4 ; isolation window 0.5 Th; normalized collision energy (NCE) 35; maximum injection time 35 ms). Monoisotopic peak assignment was used, precursor fit filter was used (70% for a fit window of 0.5 Th) and previously interrogated precursors were excluded using a dynamic window (180 $s \pm 10$ ppm). Following the acquisition of each MS₂ spectrum, a synchronous-precursor-selection (SPS) API-MS₃ scan was collected on the top 10 most intense ions b or y-ions matched by the online search algorithm in the associated MS₂ spectrum^{70,71}. MS₃ precursors were fragmented by high energy collision-induced dissociation (HCD) and analyzed using the Orbitrap (NCE 45; AGC 2.5×10^5 ; maximum injection time 200 ms, the resolution was 50,000 at 200 Th). The closeout was set at two peptides

per protein per fraction so that MS₃s were no longer collected for proteins having two peptide-spectrum matches (PSMs) that passed quality filters.

Proteomics–Phospho-proteomics analysis

Mass spectrometry data were collected using an Orbitrap Eclipse Tribrid mass spectrometer (Thermo Fisher Scientific, San Jose, CA) coupled to an UltiMate 3000 RSLCnano system liquid chromatography (LC) pump (Thermo Fisher Scientific). Peptides were separated on a 100 μ m inner diameter microcapillary column packed in-house with -30 cm of HALO Peptide ES-C18 resin (2.7 μ m, 160 \AA , Advanced Materials Technology, Wilmington, DE) over a 155 min run at -500 nL/min. For analysis, we loaded half of each fraction onto the column. Each analysis used the FAIMS Pro Interface (using previously optimized 3 CV parameters for TMT-labeled phosphopeptides) to reduce ion interference. The scan sequence began with an MS₁ spectrum (Orbitrap analysis; resolution 120,000 at 200 Th; mass range 350–1500 m/z ; automatic gain control (AGC) target 4×10^5 ; maximum injection time 50 ms). Precursors for MS₂ analysis were selected using a cycle type of 1.25 s/CV method (FAIMS CV = -40/-60/-80). MS₂ analysis consisted of high energy collision-induced dissociation (HCD) (Orbitrap analysis; resolution 50,000 at 200 Th; isolation window 0.5 Th; normalized collision energy (NCE) 38; AGC 2×10^5 ; maximum injection time 172 ms). Monoisotopic peak assignment was used, precursor fit filter was used (80% for a fit window of 0.5 Th) and previously interrogated precursors were excluded using a dynamic window (120 $s \pm 10$ ppm)⁷².

Proteomics–Data analysis

Mass spectra were processed using a Comet-based (2019.01 rev. 5) software pipeline⁷³. Spectra were converted to mzXML and monoisotopic peaks were re-assigned using Monocle⁷⁴. MS/MS spectra were matched with peptide sequences using the Comet algorithm along with a composite sequence database including the Human Reference Proteome (2020-01 - SwissProt entries only) UniProt database, as well as sequences of common contaminants. This database was concatenated with one composed of all protein sequences in the reversed order. Searches were performed using a 50 ppm precursor ion tolerance for analysis. TMT or TMTpro tags on lysine residues and peptide N termini (+229.162932 TMT; +304.207 Da TMTpro) and carbamidomethylation of cysteine residues (+57.021 Da) were set as static modifications, while oxidation of methionine residues (+15.995 Da) was set as a variable modification. For the phosphorylation dataset search, phosphorylations (+79.966 Da) on Serine or Threonine were set as additional variable modifications. Peptide-spectrum matches (PSMs) were adjusted to a 1% false discovery rate (FDR). PSM filtering was performed using a linear discriminant analysis⁷⁵, while considering the following parameters: XCorr (or Comet Log Expect), ΔC_n (or Diff Seq. Delta Log Expect), missed cleavages, peptide length, charge state, and precursor mass accuracy. For protein-level comparisons, PSMs were identified, quantified, and collapsed to a 1% peptide false discovery rate (FDR) and then collapsed further to a final protein-level FDR of 1%. Moreover, protein assembly was guided by principles of parsimony to produce the smallest set of proteins necessary to account for all observed peptides. For TMT-based reporter ion quantitation, we extracted the summed signal-to-noise (S:N) ratio for each TMT channel and found the closest matching centroid to the expected mass of the TMT reporter ion (integration tolerance of 0.003 Da). Reporter ion intensities were adjusted to correct for the isotopic impurities of the different TMT reagents according to manufacturer specifications. Proteins were quantified by summing reporter ion signal-to-noise measurements across all matching PSMs, yielding a “summed signal-to-noise” measurement. For total proteome, PSMs with poor quality, MS₃ spectra with 6 or more TMT reporter ion channels missing, or isolation specificity less than 0.8, or with TMT reporter summed signal-to-noise ratio that was less than 150 or had no MS₃ spectra were

excluded from quantification. Phosphorylation site localization was determined using the AScore algorithm. AScore is a probability-based approach for high-throughput protein phosphorylation site localization. Specifically, a threshold of 13 corresponded to 95% confidence in site localization.

Protein or peptide quantification values were exported for further analysis in Microsoft Excel, R package, and Perseus. Each reporter ion channel was summed across all quantified proteins and normalized assuming equal protein loading of all samples. Phospho-peptides were normalized to the corresponding protein abundance value (when available). Additional analysis was done using PathfindR v1.6.1, QIAGEN Ingenuity Pathway Analysis (IPA) v1.0, and PhosR v1.12R packages^{76,77}. To predict the most active kinases, we obtained the significantly upregulated phospho-peptides in the L166P dataset. We input the upregulated phospho-peptides list into kinase activity prediction tool to generate a score of activity based on based on Kim et al.⁷⁶. A detailed step-by-step guide can be found in Kim et al.⁷⁸. For the pathfindR analysis of the proteomics dataset, we included up and down-regulated proteins with a cut-off from the adjusted limma p -value of 0.05.

Supplemental data Tables list all quantified proteins as well as the associated TMT reporter ratio to control channels used for quantitative analysis.

LC-MS/MS with the hybrid metabolomics and dopamine analysis

Organoids were subjected to an LCMS analysis to detect and quantify known peaks. A metabolite extraction was carried out on each sample based on a previously described method⁷⁹. The LC column was a Millipore TMZIC-pHILIC (2.1 × 150 mm, 5 μm) coupled to a Dionex Ultimate 3000TM system and the column oven temperature was set to 25 °C for the gradient elution. A flow rate of 100 μL/min was used with the 10 mM ammonium carbonate in water (A), pH 9.0, and acetonitrile (B). The gradient profile was 80–20% B (0–30 min), 20–80% B (30–31 min), 80–80% B (31–42 min). Injection volume was set to 2 μL for all analyses (42 min total run time per injection). MS analyses were carried out by coupling the LC system to a Thermo Q Exactive HFTM mass spectrometer operating in heated electrospray ionization mode (HESI). Method duration was 30 min with polarity switching data-dependent Top 5 method for both positive and negative modes. Spray voltage for both positive and negative modes was 3.5 kV and the capillary temperature was set to 320 °C with a sheath gas rate of 35, aux gas of 10, and max spray current of 100 μA. The full MS scan for both polarities utilized 120,000 resolution with an AGC target of 3e⁶ and a maximum IT of 100 ms, and the scan range was from 67–1000 m/z . Tandem MS spectra for both positive and negative modes used a resolution of 15,000, AGC target of 1e⁵, maximum IT of 50 ms, isolation window of 0.4 m/z , isolation offset of 0.1 m/z , fixed first mass of 50 m/z , and three-way multiplexed normalized collision energies (nCE) of 10, 35, 80. The minimum AGC target was 1e4 with an intensity threshold of 2e5. All data were acquired in profile mode. The data was analyzed using the R Package and web resource <https://www.metaboanalyst.ca> MetaboAnalyst 4.0⁸⁰.

For the dopamine levels analysis, midbrain organoid samples were investigated with a reverse phase LCMS assay and dopamine was quantified across the samples. The samples were normalized by weight. Signals for dopamine were extracted by observing the peak height at m/z 154.0863. A background thresholding of 3 times the background signal plus 10,000 counts was used to determine the detection of dopamine in each sample. Finally, instrument performance was assessed using the internal standards added to the samples during extraction. Instrument mass accuracy was within tolerance (0.2 ppm), LC column performance was stable (0.39 min RT range) and internal standard response variability was 25% across the samples.

Glycolysis stress test

Organoids were submitted to the glycolysis stress test in the Agilent Seahorse XF using the glycolysis stress test. Organoids were plated in a laminin-coated Seahorse XFe96 Spheroid Microplate on day 35 and analyzed on day 40 or day 200 after plating. The assays were done in XF base medium supplemented with B27 and N2. The data was acquired using the Seahorse Wave Desktop Software 2.6.1.

Statistical analysis

All data were expressed in mean ± SEM. The statistical analysis was performed using Prism 9 (GraphPad) unless stated differently in the appropriate method section and the figures were created using Adobe Illustrator v 28. After experimental design appropriate null hypothesis testing and mean comparison, P values of <0.05 were considered significant. No statistical method was used to determine the sample size.

Reporting summary

Further information on research design is available in the Nature Portfolio Reporting Summary linked to this article.

Data availability

The MS proteomics data have been deposited to the MassIVE repository with the dataset identifier MSV000090202. The data can be accessed directly via the link <https://doi.org/10.25345/C5BV7B05F>. The metadata of the experimental cases is described in STable 3. The metabolomics is submitted at the NIH Common Fund's National Metabolomics Data Repository (NMDR) website, the Metabolomics Workbench, <https://www.metabolomicsworkbench.org> where it has been assigned Project ID (PRO01491). The data can be accessed directly via its Project DOI: (<https://doi.org/10.21228/M80M7R>). Source data are provided as a Source Data file. Source data are provided with this paper.

Code availability

The analysis code is available at <https://github.com/blanchardlab/Parfitt2023>

References

1. Reeve, A., Simcox, E. & Turnbull, D. Ageing and Parkinson's disease: why is advancing age the biggest risk factor? *Ageing Res. Rev.* **14**, 19–30 (2014).
2. Chaudhuri, J. et al. The role of advanced glycation end products in aging and metabolic diseases: bridging association and causality. *Cell Metabolism* **28**, 337–352 (2018).
3. Billingsley, K. J., Bandres-Ciga, S., Saez-Atienzar, S. & Singleton, A. B. Genetic risk factors in Parkinson's disease. *Cell Tissue Res.* **373**, 9–20 (2018).
4. Schneider, S. A., Hizli, B. & Alcalay, R. N. Emerging targeted therapeutics for genetic subtypes of Parkinsonism. *Neurotherapeutics* **17**, 1378–1392 (2020).
5. Stojkowska, I. et al. Rescue of α-synuclein aggregation in Parkinson's patient neurons by synergistic enhancement of ER proteostasis and protein trafficking. *Neuron* <https://doi.org/10.1016/j.neuron.2021.10.032> (2021).
6. Bonifati, V. et al. Mutations in the DJ-1 Gene Associated with Autosomal Recessive Early-Onset Parkinsonism. *Science* <http://science.sciencemag.org/> (2003).
7. Lockhart, P. J. et al. DJ-1 mutations are a rare cause of recessively inherited early onset parkinsonism mediated by loss of protein function. *J. Med. Genet.* **127**, e22 (2004).
8. Bandopadhyay, R. et al. The expression of DJ-1 (PARK7) in normal human CNS and idiopathic Parkinson's disease. *Brain* **127**, 420–430 (2004).

9. Canet-Avilés, R. M. et al. The Parkinson's disease DJ-1 is neuroprotective due to cysteine-sulfinic acid-driven mitochondrial localization. *Proc. Natl Acad. Sci. USA* **101**, 9103–9108 (2004).
10. Zhou, W., Zhu, M., Wilson, M. A., Petsko, G. A. & Fink, A. L. The oxidation state of DJ-1 regulates its chaperone activity toward α -Synuclein. *J. Mol. Biol.* **356**, 1036–1048 (2006).
11. Andreeva, A. et al. The apparent deglycase activity of DJ-1 results from the conversion of free methylglyoxal present in fast equilibrium with hemithioacetals and hemiaminals. *J. Biol. Chem.* **294**, 18863–18872 (2019).
12. Hasim, S. et al. A glutathione-independent glyoxalase of the DJ-1 superfamily plays an important role in managing metabolically generated methylglyoxal in candida albicans. *J. Biol. Chem.* **289**, 1662–1674 (2014).
13. Jun, Y. W. & Kool, E. T. Small substrate or large? debate over the mechanism of glycation adduct repair by DJ-1. *Cell Chem. Biol.* **27**, 1117–1123 (2020).
14. Richarme, G. et al. Parkinsonism-associated protein DJ-1/park7 is a major protein deglycase that repairs methylglyoxal- and glyoxal-glycated cysteine, arginine, and lysine residues. *J. Biol. Chem.* **290**, 1885–1897 (2015).
15. Richarme, G. et al. Guanine glycation repair by DJ-1/ Park7 and its bacterial homologs. *Science* **357**, 208–211 (2017).
16. Sharma, N., Rao, S. P. & Kalivendi, S. V. The deglycase activity of DJ-1 mitigates α -synuclein glycation and aggregation in dopaminergic cells: Role of oxidative stress mediated downregulation of DJ-1 in Parkinson's disease. *Free Radic. Biol. Med.* **135**, 28–37 (2019).
17. Ahfeldt, T. et al. Pathogenic pathways in early-onset autosomal recessive Parkinson's disease discovered using isogenic human dopaminergic neurons. *Stem Cell Rep.* **14**, 75–90 (2020).
18. Burbulla, L. F. et al. Dopamine oxidation mediates mitochondrial and lysosomal dysfunction in Parkinson's disease. *Science* **357**, 1255–1261 (2017).
19. Surmeier, D. J., Obeso, J. A. & Halliday, G. M. Selective neuronal vulnerability in Parkinson disease. *Nat. Rev. Neurosci.* **18**, 101–113 (2017).
20. Nalls, M. A. et al. Imputation of sequence variants for identification of genetic risks for Parkinson's disease: a meta-analysis of genome-wide association studies. *Lancet* **377**, 641–649 (2011).
21. Song, Y. J. C. et al. Degeneration in different parkinsonian syndromes relates to astrocyte type and astrocyte protein expression. *J. Neuropathol. Exp. Neurol.* **68**, 1073–1083 (2009).
22. Tong, J. et al. Low levels of astroglial markers in Parkinson's disease: relationship to α -synuclein accumulation. *Neurobiol. Dis.* **82**, 243–253 (2015).
23. Hishikawa, N., Hashizume, Y., Yoshida, M. & Sobue, G. Widespread occurrence of argyrophilic glial inclusions in Parkinson's disease. *Neuropathol. Appl. Neurobiol.* **27**, 362–372 (2001).
24. Smajić, S. et al. Single-cell sequencing of human midbrain reveals glial activation and a Parkinson-specific neuronal state. *Brain* <https://doi.org/10.1093/brain/awab446> (2022).
25. di Domenico, A. et al. Patient-specific iPSC-derived astrocytes contribute to non-cell-autonomous neurodegeneration in Parkinson's disease. *Stem Cell Rep.* **12**, 213–229 (2019).
26. Kam, T.-I., Hinkle, J. T., Dawson, T. M. & Dawson, V. L. Microglia and astrocyte dysfunction in Parkinson's disease. *Neurobiol. Dis.* **144**, 105028 (2020).
27. Streubel-Gallasch, L. et al. Parkinson's disease-associated LRRK2 interferes with astrocyte-mediated alpha-synuclein clearance. *Mol. Neurobiol.* **58**, 3119–3140 (2021).
28. Tsunemi, T. et al. Astrocytes protect human dopaminergic neurons from α -synuclein accumulation and propagation. *J. Neurosci.* **40**, 8618–8628 (2020).
29. Wilson, H. et al. Imidazoline 2 binding sites reflecting astroglia pathology in Parkinson's disease: An in vivo ¹¹C-BU99008 PET study. *Brain* **142**, 3116–3128 (2019).
30. Choi, D. J. et al. A Parkinson's disease gene, DJ-1, repairs brain injury through Sox9 stabilization and astrogliosis. *Glia* **66**, 445–458 (2018).
31. De Miranda, B. R. et al. Astrocyte-specific DJ-1 overexpression protects against rotenone-induced neurotoxicity in a rat model of Parkinson's disease. *Neurobiol. Dis.* **115**, 101–114 (2018).
32. Choi, D. J., An, J., Jou, I., Park, S. M. & Joe, E. H. A Parkinson's disease gene, DJ-1, regulates anti-inflammatory roles of astrocytes through prostaglandin D 2 synthase expression. *Neurobiol. Dis.* **127**, 482–491 (2019).
33. Jo, J. et al. Midbrain-like organoids from human pluripotent stem cells contain functional dopaminergic and neuromelanin-producing neurons. *Cell Stem Cell* **19**, 248–257 (2016).
34. Mohamed, N.-V. et al. Midbrain organoids with an SNCA gene triplication model key features of synucleinopathy. *Brain Commun.* **3**, 1–21 (2021).
35. Pantazis, C. B. et al. A reference human induced pluripotent stem cell line for large-scale collaborative studies. *Cell Stem Cell* **29**, 1685–1702.e22 (2022).
36. Sarrafha, L. et al. High-throughput generation of midbrain dopaminergic neuron organoids from reporter human pluripotent stem cells. *STAR Protoc.* **2**, 100463 (2021).
37. Lashuel, H. A., Overk, C. R., Oueslati, A. & Masliah, E. The many faces of α -synuclein: From structure and toxicity to therapeutic target. *Nat. Rev. Neurosci.* **14**, 38–48 (2013).
38. Oueslati, A. Implication of alpha-synuclein phosphorylation at S129 in synucleinopathies: what have we learned in the last decade? *J. Parkinsons Dis.* **6**, 39–51 (2016).
39. Mazzulli, J. R. et al. Gaucher disease glucocerebrosidase and α -synuclein form a bidirectional pathogenic loop in synucleinopathies. *Cell* **146**, 37–52 (2011).
40. Stojkowska, I. et al. Rescue of α -synuclein aggregation in Parkinson's patient neurons by synergistic enhancement of ER proteostasis and protein trafficking. *Neuron* **110**, 436–451.e11 (2022).
41. Dahl, J.-U., Gray, M. J. & Jakob, U. Protein quality control under oxidative stress conditions. *J. Mol. Biol.* **427**, 1549–1563 (2015).
42. Fleming, A. et al. The different autophagy degradation pathways and neurodegeneration. *Neuron* **110**, 935–966 (2022).
43. Takeuchi, M. & Yamagishi, S. Possible involvement of advanced glycation end-products (AGEs) in the pathogenesis of Alzheimers disease. *Curr. Pharm. Des.* **14**, 973–978 (2008).
44. Vicente Miranda, H. et al. Glycation potentiates α -synuclein-associated neurodegeneration in synucleinopathies. *Brain* **140**, 1399–1419 (2017).
45. Dalfó, E. et al. Evidence of oxidative stress in the neocortex in incidental Lewy body disease. *J. Neuropathol. Exp. Neurol.* **64**, 816–830 (2005).
46. Kierdorf, K. & Fritz, G. RAGE regulation and signaling in inflammation and beyond. *J. Leukoc. Biol.* **94**, 55–68 (2013).
47. Ioannou, M. S. et al. Neuron-astrocyte metabolic coupling protects against activity-induced fatty acid toxicity. *Cell* **177**, 1522–1535.e14 (2019).
48. Kriks, S. et al. Dopamine neurons derived from human ES cells efficiently engraft in animal models of Parkinson's disease. *Nature* **480**, 547–551 (2011).
49. Escartin, C. et al. Reactive astrocyte nomenclature, definitions, and future directions. *Nat. Neurosci.* **24**, 312–325 (2021).
50. Ciryam, P., Tartaglia, G. G., Morimoto, R. I., Dobson, C. M. & Vendruscolo, M. Widespread aggregation and neurodegenerative diseases are associated with supersaturated proteins. *Cell Rep.* **5**, 781–790 (2013).

51. Bordi, M. et al. Autophagy flux in CA1 neurons of Alzheimer hippocampus: Increased induction overburdens failing lysosomes to propel neuritic dystrophy. *Autophagy* **12**, 2467–2483 (2016).
52. Kiffin, R., Christian, C., Knecht, E. & Cuervo, A. M. Activation of Chaperone-mediated Autophagy during Oxidative Stress. *Mol. Biol. Cell* **15**, 4829–4840 (2004).
53. Radulovic, M. et al. ESCRT-mediated lysosome repair precedes lysophagy and promotes cell survival. *EMBO J.* **37**, e99753 (2018).
54. Song, W. et al. The Parkinson disease-associated A30P mutation stabilizes α -synuclein against proteasomal degradation triggered by heme oxygenase-1 over-expression in human neuroblastoma cells. *J. Neurochem.* **110**, 719–733 (2009).
55. Bourdenx, M. et al. Chaperone-mediated autophagy prevents collapse of the neuronal metastable proteome. *Cell* **184**, 2696–2714.e25 (2021).
56. Konig, A., Miranda, H. V. & Outeiro, T. F. Alpha-synuclein glycation and the action of anti-diabetic agents in Parkinson's disease. *J. Parkinson's Dis.* **8**, 33–43 (2018).
57. Yang, Y.-W. et al. Increased risk of Parkinson disease with diabetes mellitus in a population-based study. *Medicine* **96**, e5921 (2017).
58. Adamopoulos, C. et al. Advanced glycation end-products induce endoplasmic reticulum stress in human aortic endothelial cells. *Clin. Chem. Lab Med.* **52**, 151–160 (2014).
59. Raupbach, J., Ott, C., Koenig, J. & Grune, T. Proteasomal degradation of glycated proteins depends on substrate unfolding: Preferred degradation of moderately modified myoglobin. *Free Radic. Biol. Med.* **152**, 516–524 (2020).
60. Mazza, M. C. et al. DJ-1 is not a deglycase and makes a modest contribution to cellular defense against methylglyoxal damage in neurons. *J. Neurochem.* **162**, 245–261 (2022).
61. Sánchez, C., Diaz-Nido, J. & Avila, J. Phosphorylation of microtubule-associated protein 2 (MAP2) and its relevance for the regulation of the neuronal cytoskeleton function. *Prog. Neurobiol.* **61**, 133–168 (2000).
62. Kumaran, R. & Cookson, M. R. Pathways to Parkinsonism Redux: convergent pathobiological mechanisms in genetics of Parkinson's disease. *Hum. Mol. Genet.* **24**, R32–R44 (2015).
63. Bernis, M. E. et al. Prion-like propagation of human brain-derived alpha-synuclein in transgenic mice expressing human wild-type alpha-synuclein. *Acta Neuropathol. Commun.* **3**, 75 (2015).
64. Miller, D. W. et al. L166P mutant DJ-1, causative for recessive Parkinson's disease, is degraded through the ubiquitin-proteasome system. *J. Biol. Chem.* **278**, 36588–36595 (2003).
65. Olzmann, J. A. et al. Familial Parkinson's disease-associated L166P mutation disrupts DJ-1 protein folding and function. *J. Biol. Chem.* **279**, 8506–8515 (2004).
66. Rao, J. et al. ATF6 mediates a pro-inflammatory synergy between ER stress and TLR activation in the pathogenesis of liver ischemia-reperfusion injury. *Am. J. Transplant.* **14**, 1552–1561 (2014).
67. TCW, J. et al. An efficient platform for astrocyte differentiation from human induced pluripotent stem cells. *Stem Cell Rep.* **9**, 600–614 (2017).
68. Schweppe, D. K. et al. Characterization and optimization of multiplexed quantitative analyses using high-field asymmetric-waveform ion mobility mass spectrometry. *Anal. Chem.* **91**, 4010–4016 (2019).
69. McAlister, G. C. et al. MultiNotch MS3 enables accurate, sensitive, and multiplexed detection of differential expression across cancer cell line proteomes. *Anal. Chem.* **86**, 7150–7158 (2014).
70. Erickson, B. K. et al. Active instrument engagement combined with a real-time database search for improved performance of sample multiplexing workflows. *J. Proteome Res.* **18**, 1299–1306 (2019).
71. Schweppe, D. K. et al. Full-featured, real-time database searching platform enables fast and accurate multiplexed quantitative proteomics. *J. Proteome Res.* **19**, 2026–2034 (2020).
72. Schweppe, D. K., Rusin, S. F., Gygi, S. P. & Paulo, J. A. Optimized workflow for multiplexed phosphorylation analysis of TMT-labeled peptides using high-field asymmetric waveform ion mobility spectrometry. *J. Proteome Res.* **19**, 554–560 (2020).
73. Eng, J. K., Jahan, T. A. & Hoopmann, M. R. Comet: An open-source MS/MS sequence database search tool. *Proteomics* **13**, 22–24 (2013).
74. Rad, R. et al. Improved monoisotopic mass estimation for deeper proteome coverage. *J. Proteome Res.* **20**, 591–598 (2021).
75. Huttlin, E. L. et al. A tissue-specific atlas of mouse protein phosphorylation and expression. *Cell* **143**, 1174–1189 (2010).
76. Kim, H. J. et al. PhosR enables processing and functional analysis of phosphoproteomic data. *Cell Rep.* **34**, 108771 (2021).
77. Ulgen, E., Ozisik, O. & Sezerman, O. U. PathfindR: An R package for comprehensive identification of enriched pathways in omics data through active subnetworks. *Front. Genet.* **10**, 858 (2019).
78. Kim, H. J., Kim, T., Xiao, D. & Yang, P. Protocol for the processing and downstream analysis of phosphoproteomic data with PhosR. *STAR Protoc.* **2**, 100585 (2021).
79. Pacold, M. E. et al. A PHGDH inhibitor reveals coordination of serine synthesis and one-carbon unit fate. *Nat. Chem. Biol.* **12**, 452–458 (2016).
80. Chong, J., Wishart, D. S. & Xia, J. Using MetaboAnalyst 4.0 for comprehensive and integrative metabolomics data analysis. *Curr. Protoc. Bioinforma.* **68**, 1–128 (2019).

Acknowledgements

The authors thank Bill Skarnes, iPSC Neurodegenerative Disease Initiative (iNDI), the Center for Alzheimer's and Related Dementias (CARD) and the ASAP consortium for the donation of the KOLF2.1J and L166P cell lines. Deans Flow Cytometry CoRE at Icahn School of Medicine Flow Cytometry Core for discussions and technical expertise in sorting, Mount Sinai for flow cytometry training, and the Neuropathology Brain Bank & Research CoRE at the Icahn School of Medicine at Mount Sinai for the technical help in sectioning, staining, and imaging spheres. The NYU metabolomics core for help in designing and analyzing the metabolomics experiments. The study is funded by the joint efforts of The Michael J. Fox Foundation for Parkinson's Research (MJFF) and the Aligning Science Across Parkinson's (ASAP) initiative. MJFF administers the grant [O2663614] on behalf of ASAP and itself., NIH grant R01:0255E131, C.G. received a T32: 2T32AGO49688-06 grant, L.S. was supported by the Training Program in Stem Cell Biology fellowship from the New York State Department of Health (NYSTEM-C32561GG). Work in A.O.'s laboratory is supported by Sloan Kettering Institute startup funds, the Pew Charitable Trusts, and the Basic Science Research Program through the National Research Foundation of Korea (NRF) funded by the Ministry of Education (2021R1A6A3A14038416 to K.H.N.). This research was also in part supported by the Memorial Sloan Kettering Cancer Center Support Grant P30CA008748 (A.O.).

Author contributions

G.M.P., T.D.A., and J.B. designed the experiments and wrote the manuscript with input of all authors. G.M.P., E.C., L.S., C.G., R.R., and S.S. performed the tissue culture experiments and contributed with data analysis. D.J. contributed with technical expertise and data interpretation for the metabolomics experiments. K.H.N. and A.O. contributed with technical expertise and data interpretation for the proteomics experiments. J.F.C. and K.W. contributed with the design, data analysis, and interpretation of human tissue experiments.

Competing interests

The authors declare no competing interests.

Additional information

Supplementary information The online version contains supplementary material available at <https://doi.org/10.1038/s41467-024-44732-2>.

Correspondence and requests for materials should be addressed to Gustavo Morrone Parfitt, Joel Blanchard or Tim Ahfeldt.

Peer review information *Nature Communications* thanks Antonella Consiglio and the other, anonymous, reviewers for their contribution to the peer review of this work.

Reprints and permissions information is available at <http://www.nature.com/reprints>

Publisher's note Springer Nature remains neutral with regard to jurisdictional claims in published maps and institutional affiliations.

Open Access This article is licensed under a Creative Commons Attribution 4.0 International License, which permits use, sharing, adaptation, distribution and reproduction in any medium or format, as long as you give appropriate credit to the original author(s) and the source, provide a link to the Creative Commons license, and indicate if changes were made. The images or other third party material in this article are included in the article's Creative Commons license, unless indicated otherwise in a credit line to the material. If material is not included in the article's Creative Commons license and your intended use is not permitted by statutory regulation or exceeds the permitted use, you will need to obtain permission directly from the copyright holder. To view a copy of this license, visit <http://creativecommons.org/licenses/by/4.0/>.

© The Author(s) 2024